Article

Molecular Cell

Single-Molecule Analysis Reveals Linked Cycles of RSC Chromatin Remodeling and Ace1p Transcription Factor Binding in Yeast

Graphical Abstract

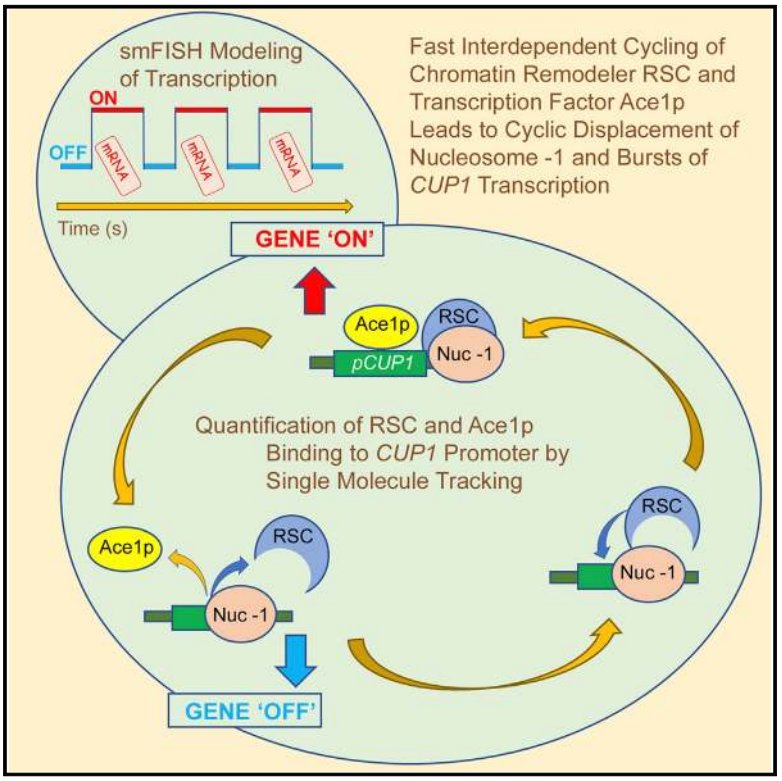

Highlights

- SMT and smFISH reveal the link between chromatin remodeling and TF binding
- Cycles of TF Ace1p binding at the promoter lead to transcription bursts of *CUP1*
- *CUP1* transcription bursts depend on short cycles of nucleosome mobilization by RSC
- RSC ensures a homogeneous response of the cell population to heavy metal stress

Authors

Gunjan D. Mehta, David A. Ball, Peter R. Eriksson, Razvan V. Chereji, David J. Clark, James G. McNally, Tatiana S. Karpova

Correspondence

karpovat@mail.nih.gov

In Brief

In this study, Mehta et al. show that rapid cycles of the yeast transcription factor Ace1p at *CUP1* promoter serve as a pacemaker for the transcription bursts. The chromatin remodeler RSC fine-tunes this cycle by short repetitive cycles of nucleosome mobilization.

Mehta et al., 2018, Molecular Cell *72*, 875–887
December 6, 2018 Published by Elsevier Inc.
https://doi.org/10.1016/j.molcel.2018.09.009

Molecular Cell
Article

Single-Molecule Analysis Reveals Linked Cycles of RSC Chromatin Remodeling and Ace1p Transcription Factor Binding in Yeast

Gunjan D. Mehta,[1] David A. Ball,[1] Peter R. Eriksson,[2] Razvan V. Chereji,[2] David J. Clark,[2] James G. McNally,[3] and Tatiana S. Karpova[1,4,*]

[1]CCR/LRBGE Optical Microscopy Core, National Cancer Institute, National Institutes of Health, Bethesda, MD 20892, USA
[2]Division of Developmental Biology, Eunice Kennedy Shriver National Institute for Child Health and Human Development, National Institutes of Health, Bethesda, MD 20892, USA
[3]Institute for Soft Matter and Functional Materials, Helmholtz Center Berlin, Berlin 12489, Germany
[4]Lead Contact
*Correspondence: karpovat@mail.nih.gov
https://doi.org/10.1016/j.molcel.2018.09.009

SUMMARY

It is unknown how the dynamic binding of transcription factors (TFs) is molecularly linked to chromatin remodeling and transcription. Using single-molecule tracking (SMT), we show that the chromatin remodeler RSC speeds up the search process of the TF Ace1p for its response elements (REs) at the *CUP1* promoter. We quantified smFISH mRNA data using a gene bursting model and demonstrated that RSC regulates transcription bursts of *CUP1* only by modulating TF occupancy but does not affect initiation and elongation rates. We show by SMT that RSC binds to activated promoters transiently, and based on MNase-seq data, that RSC does not affect the nucleosomal occupancy at *CUP1*. Therefore, transient binding of Ace1p and rapid bursts of transcription at *CUP1* may be dependent on short repetitive cycles of nucleosome mobilization. This type of regulation reduces the transcriptional noise and ensures a homogeneous response of the cell population to heavy metal stress.

INTRODUCTION

Many transcription factors (TFs) bind to specific response elements (REs) with dynamics on the scale of seconds (Voss and Hager, 2014). Biophysical data suggest that fast exchange is a mechanism for optimization of gene activation (Clauß et al., 2017; Lickwar et al., 2012; Stavreva et al., 2004; Van Royen et al., 2014). However, little is known about the regulation of TF transient binding. Chromatin remodelers move and disassemble nucleosomes (Bowman and McKnight, 2017) and were also shown to evict the TF by inducing collisions between a nucleosome and the TF *in vitro* (Li et al., 2015). Thus, it is plausible that chromatin remodeling may affect TF dynamics. However, nothing is known at the molecular level about the links between *in vivo* remodeling and TF binding. Single-molecule tracking (SMT) is a method of choice to quantify *in vivo* molecular dynamics (Ball et al., 2016; Izeddin et al., 2014; Mazza et al., 2013). However, SMT quantifications are predominantly based on averaging of the data obtained for a population of REs present in the whole nucleus, and this may obscure the variability in binding parameters of a TF and its underlying regulatory mechanisms. We characterized by SMT the binding of a TF to a specific promoter. We employed a yeast model consisting of the metallothionein-encoding *CUP1* and its copper-dependent transcription activator, Ace1p (Fürst et al., 1988). Fast cycling of Ace1p at the promoter of *CUP1* was previously demonstrated by FRAP and CLK-ChIP (Karpova et al., 2008; Poorey et al., 2013). Activation of *CUP1* correlates with a loss of histones (Karpova et al., 2008) and leads to an Ace1p-dependent switch from positioned nucleosomes to a fluid chromatin structure (Shen et al., 2001). By SMT of Ace1p, we demonstrated that the chromatin remodeler complex RSC improves the search of Ace1p for its REs at the *CUP1* promoter by increasing (1) the fraction of accessible REs and (2) the molecular "on" rate of Ace1p binding. Contrary to other systems, where transcription is improved by an increase in TF residence time (Loffreda et al., 2017; Morisaki et al., 2014; Paakinaho et al., 2017), *CUP1* improvement in transcription correlates with decrease in Ace1p residence time. To quantify the effect of RSC on transcription, we analyzed the smFISH of *CUP1* mRNA using a standard model for bursting gene expression. Parameter estimates produced by the model indicate that RSC has no effect on transcription initiation and elongation rates, and changes in transcription induced by RSC may be explained completely by its effect on TF binding. Thus, we have demonstrated how nucleosome displacement by itself can alter transcription dynamics. Consequently, RSC increases the fraction of active cells, reduces the transcriptional noise, and ensures a homogeneous response of the cell population to heavy metal stress. As observed by SMT, RSC binds to an activated *CUP1* promoter transiently. Based on MNase-seq data, the rapid cyclical activity of RSC does not affect nucleosomal occupancy at *CUP1*. Our results are summarized in a model proposing that transcription bursts at *CUP1* depend on short, repetitive TF binding and rapid, repetitive chromatin remodeling.

RESULTS

Assay for Specific Binding of Ace1p to Activated Promoters of *CUP1*

CUP1 encoding yeast metallothionein forms a 10× natural tandem array in yeast *Saccharomyces cerevisiae* (Zhao et al., 2014). We performed SMT of Ace1p-HaloTag labeled with JF_{646} (Grimm et al., 2015) at the *CUP1* promoter in cells activated with 100 μM Cu^{2+}. Promoters were visualized by Ace1p-3xGFP (Karpova et al., 2008) (Figure 1A and Movie S1). As a control, we also tracked Ace1p over the *lacO* array, observed by the binding of *LacI*-GFP, as it has no known binding sites for Ace1p (Figure 1B and Movie S2). We confirmed that all the genetically modified strains for our experiments behave like a wild-type strain in terms of expression levels of *ACE1* and *CUP1* and their sensitivity to copper (Figure S1 and Tables S1, S2, and S3). Binding parameters were estimated from survival times of Ace1p (Ball et al., 2016). We plotted a histogram of the times that Ace1p molecules resided over the *CUP1* array and the *lacO* array (Figure 1C). An exponential fit of the distribution of Ace1p survival at *CUP1* yielded two binding states with mean residence times of 0.59 ± 0.05 s and 2.96 ± 0.26 s (Figures 1C and 1D). At *lacO* we observed only a single fraction of Ace1p-bound molecules with residence time comparable to that for short-residence Ace1p on *CUP1* (0.78 ± 0.05 s). Therefore, the short residence times of Ace1p most likely reflect non-specific binding, while the longer residence times observed only at *CUP1* reflect specific binding. The tracking method and residence time analysis based on the survival distribution is explained in the Method Details (Figure S2).

RSC Affects Transient-Specific Binding of Ace1p at *CUP1* Promoter

In yeast, specificity of binding of the RSC complex is determined by the mutually exclusive and non-essential subunits Rsc1p and Rsc2p (Cairns et al., 1999). Only Rsc2p, not Rsc1p, affects Ace1p binding (Karpova et al., 2004). Therefore, we tested the effects of Rsc2p on the specific binding of Ace1p to the RE of the *CUP1* promoter in conditions of Rsc2p depletion. We took advantage of the auxin-inducible degron (AID) system (Morawska and Ulrich, 2013; Nishimura et al., 2009) for the conditional depletion of Rsc2p and characterized this system in our experimental strain (YTK1649) as described in Method Details (Figure S3). The specific bound fraction of Ace1p is reduced 2.5× in $Rsc2^-$ cells (3.8% ± 0.8%) in comparison with $Rsc2^+$ cells (10.4% ± 2.6%, $p < 0.001$) (Figure 2A). Similarly, the specific bound fraction of Ace1p is reduced in *rsc2*Δ (2.7% ± 1.2%) in comparison with *RSC2* (14.5% ± 1.8%) (Figure 2B). Wild-type *RSC2* introduced into $Rsc2^-$ cells compensates for the depletion of the endogenous Rsc2p and restores the specific bound fraction of Ace1p to 12.1% ± 4.1% (Figure 2C).

RSC Associates with Active *CUP1* Locus and Modulates Its Transcription and Copper Sensitivity of the Cells

Using ChIP, we detected a 60% increase in the accumulation of Rsc2p at activated *CUP1* (Figure 3A). Using qPCR estimates, depletion of Rsc2p leads to a ~30% reduction in transcription of *CUP1* and to higher copper sensitivity (Figures 3B and 3C). Thus, the effect of the RSC complex on Ace1p binding correlates with an improvement in *CUP1* transcription and cell survival in the presence of copper. Surprisingly, contrary to other systems, Ace1p residence time increases in $Rsc2^-$ cells even though *CUP1* transcription is reduced (Figures 2A, 2B, and 2D).

RSC Affects the Search of Ace1p for Its Specific RE

The molecular mechanism of RSC action may be deduced from the SMT estimates of Ace1p binding. The bound fraction of Ace1p (C_{eq}), defined as the ratio of bound to total molecules, depends on the residence time and on the search time of Ace1p for an RE at *CUP1*, as described simplistically by Equation 1:

$$C_{eq} = \frac{C_{bound}}{C_{bound} + C_{free}} = \left(1 + \frac{\tau_{search}}{\tau_{res}}\right)^{-1}. \qquad \text{Equation 1}$$

The full version of Equation 1 for the case of the two binding states observed for Ace1p, both short and long, is given in Method Details, Equation M1. Therefore, an increase in C_{eq}, observed as a higher occupancy of the RE by TF, may result from: (1) decrease in the availability of the TF, C_{free}; (2) decrease in the dissociation rate, k_{off}; (3) increase in the availability of the RE, S_{eq}; or (4) increase in the association rate, k_{on}. Based on our data, we can eliminate the first two causes. First, there is no difference in total nuclear Ace1p for $Rsc2^+$ and $Rsc2^-$ cells (Figure S3D). Second, $\tau_{res} = 1/k_{off}$ decreases rather than increases in $Rsc2^+$ cells. Thus, the increase in C_{eq} observed in $Rsc2^+$ cells must be due to a decrease in the search time. From the estimates for the ratio of C_{eq} and τ_{res} obtained from SMT for the full two-state binding model (Equation M6), τ_{search} is ~8 s ($Rsc2^+$) and ~25 s ($Rsc2^-$). Therefore, RSC speeds up the search of Ace1p for *CUP1* REs, by an increase in either the molecular "on" rate for Ace1p (k_{on}) and/or the concentration of free REs for *CUP1* (S_{eq}), as given by:

$$\tau_{search} = k_{on}^{*-1} = (k_{on} S_{eq})^{-1}. \qquad \text{Equation 2}$$

RSC Affects the "On" Rate of Ace1p and the Availability of RE at *CUP1* Promoter

Estimates of the relative impact of k_{on} and S_{eq} may shed light on the molecular mechanism of RSC action. Although both parameters are dependent on the presence of nucleosome-free DNA at the promoter, they depend on slightly different conditions: S_{eq} indicates how many REs are free from nucleosomes, and k_{on} is dependent on the size of the target for the search (Mirny et al., 2009). Predominant regulation of S_{eq} indicates that the area free of nucleosomes may be relatively small, covering only the RE, but predominant regulation of k_{on} indicates that this area should be larger than the RE. However, SMT allows direct estimation of only k^*_{on}. S_{eq} may be estimated from the fraction of non-activated *CUP1* in the cell population, F_{nt}. If we assume that binding of Ace1p to any of the four REs in the *CUP1* gene occurs equally and independently and results in transcription, then we can relate F_{nt} to the probability, P, that any one RE is available as described by Method Details Equation M8. From the calculated probability of each RE being available, and providing four REs exist per promoter, we end up with an average number of

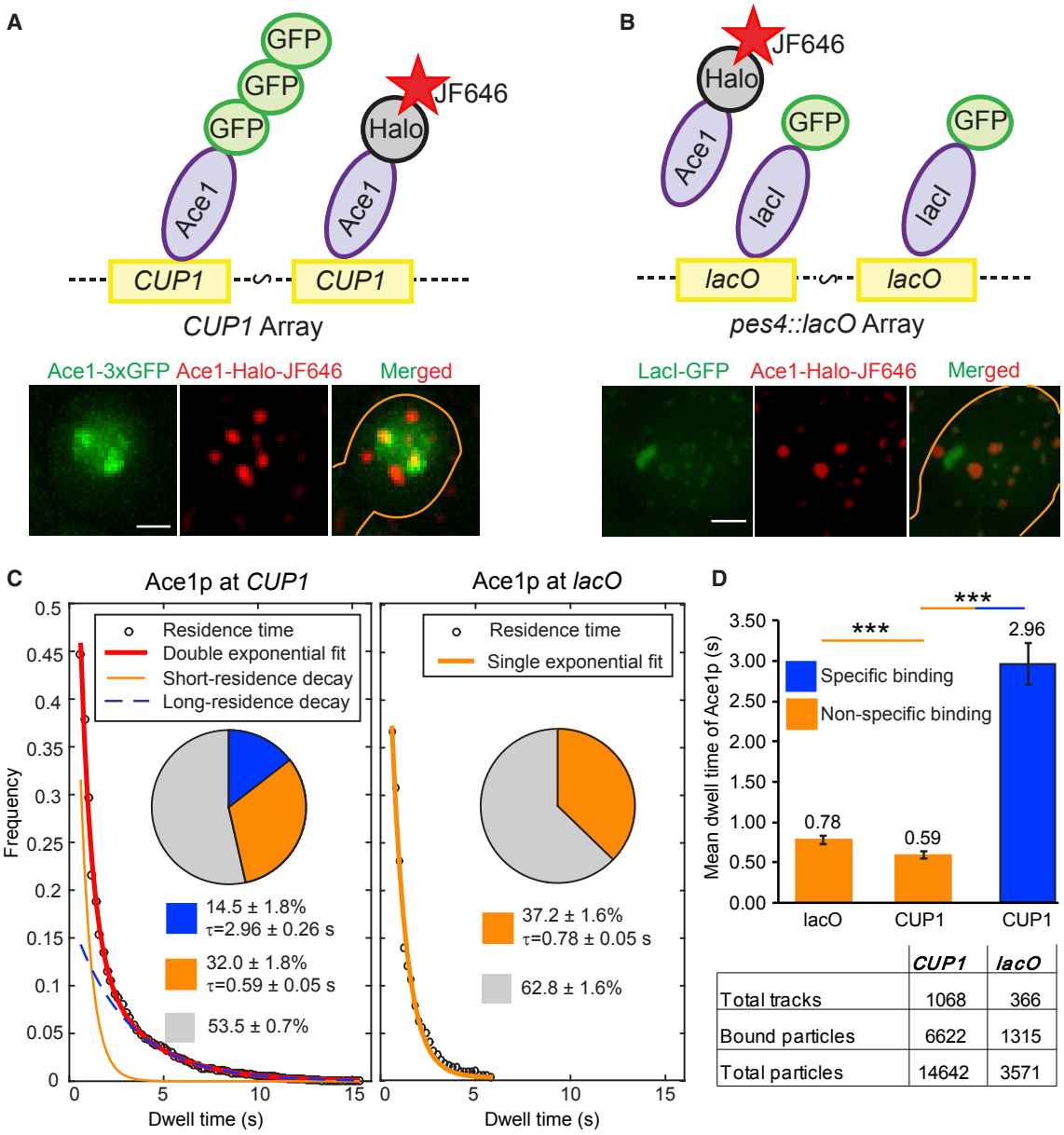

	CUP1	lacO
Total tracks	1068	366
Bound particles	6622	1315
Total particles	14642	3571

Figure 1. Assay for Specific Binding of Ace1p to Activated Promoters of *CUP1*

Figure360▷ For a Figure360 author presentation of Figure 1, see https://doi.org/10.1016/j.molcel.2018.09.009.

(A and B) Ace1p-3xGFP (A) at the *CUP1* array in YTK1498 or GFP-lacI (B) at *pes4::LacO* array in YTK1528 define the site for tracking of the individual molecules of Ace1p-HaloTag labeled with JF_{646} at a low density of $\leq$ 5 particles per nucleus. Molecules of Ace1p-HaloTag (JF_{646}) frequently colocalize with *CUP1* array and rarely colocalize with *lacO* array, as demonstrated by single-focal-plane representative images. Gaussian filter was applied to Ace1p-HaloTag (JF_{646}) channel in Track Record software for better visualization of the particles. Here and in Figures 4B and 4C, brightness and contrast were adjusted using linear LUT in ImageJ and cell contours were drawn manually in Adobe Illustrator. Scale bar, 2 μm. See also Videos S1 and S2.

(C) Raw distributions of survival of Ace1p particles are shown with the exponential decay fits. For this and Figures 2 and 6A, pie charts represent the extracted distributions of diffusing (gray), specific (blue), and non-specific (orange) binding events with their average residence times; the table shows the number of molecules/tracks observed for a particular sample.

(D) The difference between residence times of Ace1p. ***$p < 0.001$ by z test. Error bars indicate SEM.

available REs, and therefore we may calculate S_{eq} based on Avogadro's number N_A and the volume of the yeast nucleus V, as described by Equation M9. From Equation 2 we may then calculate k_{on}.

Estimation of F_{nt} is complicated by the presence of ten copies of *CUP1* in each array, because transcripts observed in individual cells may be produced from any number of active *CUP1*. To observe transcription of just a single copy of *CUP1* per cell by

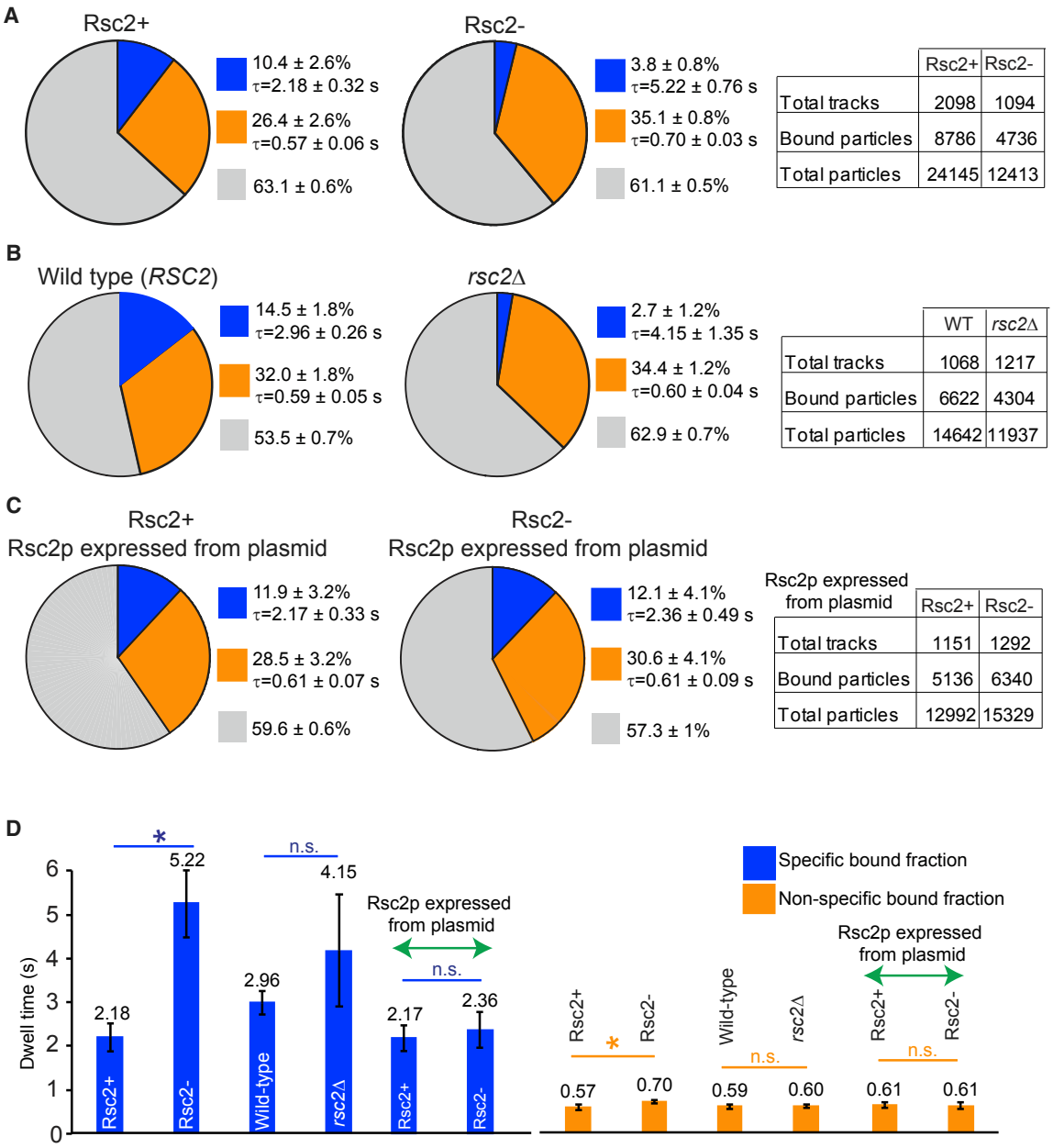

Figure 2. RSC Affects Transient Binding of Ace1p at *CUP1* Promoter

(A and B) SMT of Ace1p at *CUP1*; charts, graphs, and tables as described in the caption to Figure 1. Effect of Rsc2p depletion (A, YTK1649) or *rsc2* knockout (B, YTK1526 versus WT YTK1498) on Ace1p binding at *CUP1* is shown.

(C) Compensation for depletion of Rsc2p by Rsc2p expressed from centromeric plasmid in YTK1582.

(D) The average residence time of Ace1p at *CUP1* from (A)–(C). n.s., not significant; $0.09 < p < 0.94$, $^*p < 0.05$ by z test. Error bars indicate SEM.

smFISH, we replaced the ORF of a single *CUP1* gene within the array by an artificial sequence (*CUP1* reporter) (Figures 4A and S4). In the diploid tested, only one of the arrays contained the reporter (Figure 4B). We characterized and validated the use of *CUP1* reporter as an adequate test for the expression of the entire *CUP1* array (Figure S5). The following conclusions are based on the assumption that all promoters in both arrays and in all the cells perform independently.

We observed that in the control group not treated with Cu^{2+}, cells contain on average very few mature mRNA of the *CUP1* reporter (0.46 ± 0.03 [SEM]) per cell, with a maximum of 8 (Figure 4C). Cells that do not contain any mRNA constituted 67.2% of the whole population. The histogram of mature mRNA per cell is fit well to a Poisson distribution, indicating that basal expression of *CUP1* is governed by random, uncoordinated initiation, rather than a bursting behavior (Figure 4D, upper panel).

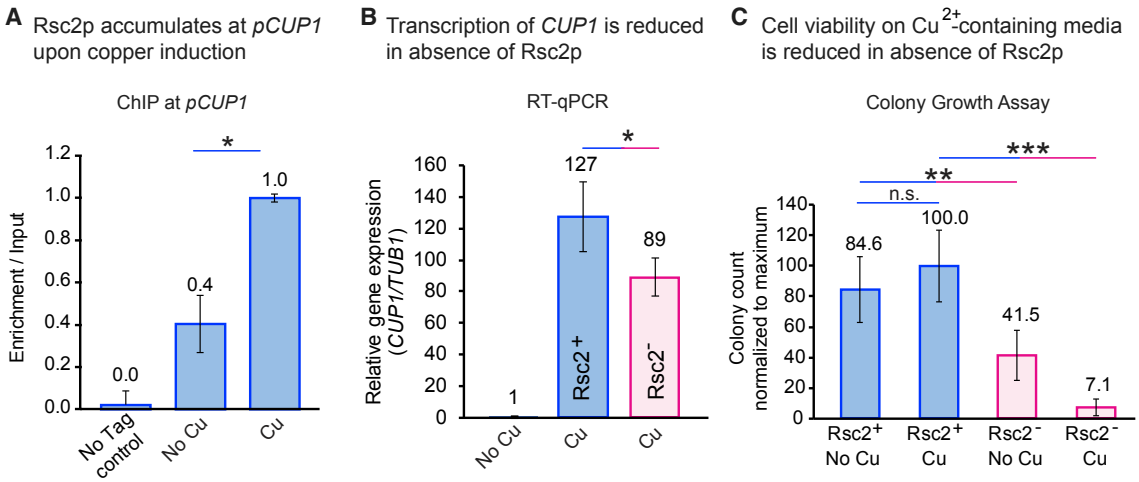

Figure 3. RSC Associates with Active *CUP1* Locus and Modulates Its Transcription and Copper Sensitivity of the Cells

(A) Binding of Rsc2p-AID*-9Myc to promoters of *CUP1* upon activation with copper was assayed by ChIP.

(B and C) The effect of Rsc2p depletion on transcription of *CUP1* was quantified by RT-qPCR (B) and on copper sensitivity of the cells by colony growth assay (C). *p < 0.05, **p < 0.01, ***p < 0.001 by t test. Error bars indicate SEM.

In the cells from the *CUP1* reporter sample that were treated with Cu^{2+}, both $Rsc2^+$ and $Rsc2p^-$, the same Poisson distribution (mean = 0.46) can be used to fit the initial points of the distribution of mature mRNA if it is first scaled by a constant factor, α, as described by Method Details Equation M7, indicating that the initial part of the distribution contains cells that are not transcribing above the basal level. Therefore, this fit represents the cells in which the *CUP1* reporter is not activated, and the cells treated with Cu^{2+} contain two distinct sub-populations, one of which is similar to that observed in the population of non-activated cells and can provide an estimate of F_{nt}. The fittings of this scaled Poisson to the $Rsc2^+$ and $Rsc2^-$ mRNA data are shown in the middle and lower panels of Figure 4D, respectively, and the fraction of non-activated cells is highlighted in blue in Figure 4E. Upon depletion of Rsc2p, the fraction of non-active cells, F_{nt}, in $Rsc2^-$ is roughly twice that of $Rsc2^+$, going from 14.4% ± 2.9% to 27.5% ± 11.0%. The calculated probability of an RE being available (P) is 0.38 ± 0.08 for $Rsc2^+$ and 0.28 ± 0.11 for $Rsc2^-$ cells (Table 1). Providing four REs exist per *CUP1* promoter, we end up with an average number of available REs per promoter, n = 1.54 for $Rsc2^+$ and n = 1.10 for $Rsc2^-$ (Table 1). Therefore, Rsc2p stimulates the availability of the REs. From Equation M9, for $Rsc2^+$ S_{eq} = 0.61 ± 0.13 nM, and for $Rsc2^-$ S_{eq} = 0.44 ± 0.18 nM. From S_{eq} and k^*_{on} (see Equation 2), we can estimate the molecular binding rates as 0.21 ± 0.07 nM^{-1} s^{-1} for $Rsc2^+$ and 0.12 ± 0.06 nM^{-1} s^{-1} for $Rsc2^-$. Thus, both k_{on} and S_{eq} must change to produce the change in transcription between $Rsc2^+$ and $Rsc2p^-$ cell populations. Also, in Monte Carlo simulations of TF binding, it is impossible to obtain the differences observed experimentally in $Rsc2^-$ and $Rsc2^+$ cells if only one of these parameters is affected (Figure S6 and Method Details). RSC must affect both k_{on} and S_{eq} to speed up the search of Ace1p for *CUP1* binding sites.

RSC Complex Modulates *CUP1* Transcription by Affecting Ace1p Binding

Potentially, chromatin remodeling induced by RSC may affect any or all stages of transcription, namely preinitiation, initiation, and elongation (Figure 5A). Our hypothesis is that the binding of Ace1p is necessary and sufficient to switch the gene to the "ON" state. Specifically, we make two assumptions: (1) the fraction of Ace1p productively binding to *CUP1* promoter is the fraction defined as specifically bound by SMT, and (2) the switch of *CUP1* to the "ON" state is triggered by productive binding of at least one Ace1p molecule to the promoter. Therefore, the gene "OFF" rate may be described by the Ace1p residence time, and the gene "ON" rate may be described by k_{on} and S_{eq} of Ace1p. Binding of Ace1p triggers the formation of the preinitiation complex (PIC). Downstream events such as the initiation, elongation, and degradation are not directly related to Ace1p binding. Thus, in the "ON" state the gene becomes competent for transcription; however, this state does not always lead to the formation of mature mRNA.

We applied to smFISH a model for bursting gene expression in which a gene can switch between an "ON" and an "OFF" state but can only transition to the "ON" state if at least one of its REs is available. The gene may be "ON" (active) even if no transcripts are detected. In the "ON" state, transcription may be randomly initiated, and the mRNA elongates. Finally, mature mRNA is allowed to degrade. Therefore, the transcript levels are determined by the number of bursts and burst amplitude (dependent on the amount of time that the gene is "ON" and the probability that the gene is accessible) and the rates of initiation, elongation, and degradation (Figure 5B) (Raj et al., 2006; Senecal et al., 2014; Zenklusen et al., 2008). If RSC acts only through the modulation of TF binding, we expect that changes in the levels of Rsc2p will affect the burst duration and the burst frequency but not the transcription initiation rate, k_{tx}, or production time, t_{prod} (Figures 5A and 5B).

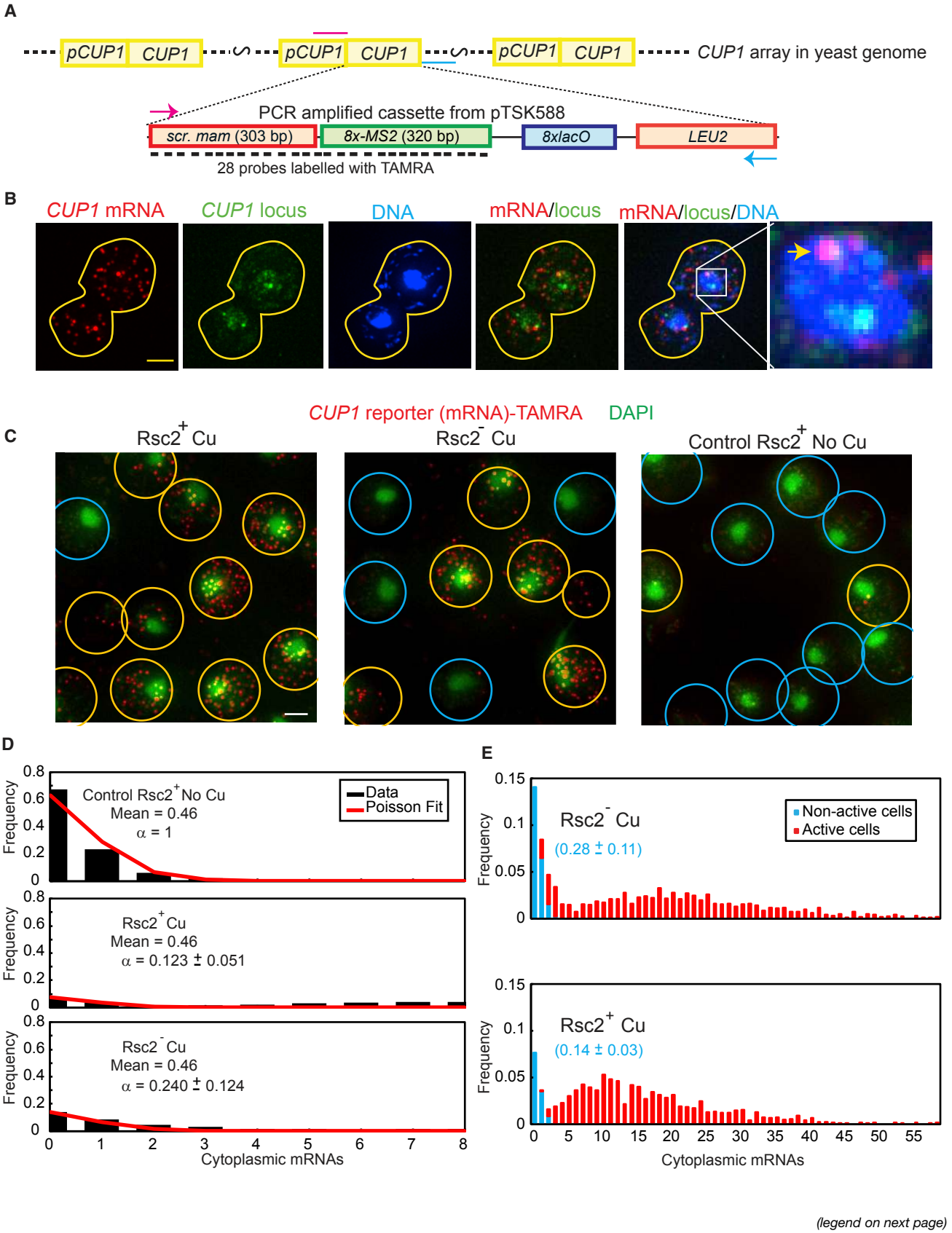

(legend on next page)

Table 1. Comparison of Direct Measurements and Transcription Model Predictions for the Parameters for *CUP1* Transcription and Ace1p Binding

Parameter Name	Rsc2$^-$	Rsc2$^+$	p value
t_{search} (s)	25 ± 3.8[a]	7.6 ± 2.0[a]	<0.001[a]
τ_{res} (s)	5.22 ± 0.76[a]	2.18 ± 0.33[a]	<0.001[a]
REs available per gene	1.10 ± 0.44[a], 0.99 ± 0.06[d]	1.54 ± 0.32[a], 1.49 ± 0.04[d]	0.11[a], <0.001[d]
k_{off} (s^{-1})	0.19 ± 0.03[b]	0.46 ± 0.07[b]	<0.001[b]
k^*_{on} (s^{-1})	0.05 ± 0.01[a], 0.05 ± 0.01[d]	0.16 ± 0.05[a], 0.12 ± 0.04[d]	<0.001[a], <0.001[d]
S_{eq} (nM)	0.44 ± 0.18[a], 0.39 ± 0.02[d]	0.61 ± 0.13[a], 0.59 ± 0.01[d]	0.13[a], <0.001[d]
k_{on} (nM^{-1} s^{-1})	0.12 ± 0.06[a], 0.14 ± 0.01[d]	0.21 ± 0.07[a], 0.21 ± 0.02[d]	0.012[a], <0.001[d]
P_{RE}	0.28 ± 0.11[a], 0.25 ± 0.02[d]	0.38 ± 0.08[a], 0.37 ± 0.01[d]	0.15[a], <0.001[d]
k_{tx} (s^{-1})	0.24 ± 0.08[c], 0.20 ± 0.02[d]	0.18 ± 0.03[c], 0.23 ± 0.05[d]	0.17[c], 0.28[d]
t_{prod} (s)	80.9 ± 43.5[c], 84.9 ± 30.8[d]	70.2 ± 21.0[c], 76.2 ± 6.2[d]	0.68[c], 0.60[d]
k_{deg} (s^{-1})	2.03 × 10^{-3} ± 0.38 × 10^{-3} [b]	2.03 × 10^{-3} ± 0.38 × 10^{-3} [b]	1[b]
Burst frequency (s^{-1})	0.04 ± 0.01[c], 0.04 ± 0.003[d]	0.12 ± 0.03[c], 0.10 ± 0.02[d]	<0.001[c], <0.001[d]
Burst duration (s)	5.22 ± 0.76[a]	2.18 ± 0.33[a]	<0.001[a]
Burst amplitude (mRNA/burst)	1.28 ± 0.47[c], 1.06 ± 0.19[d]	0.39 ± 0.09[c], 0.52 ± 0.14[d]	<0.001[c], <0.001[d]

Errors represent 95% confidence intervals.
[a]Parameters derived from the directly measured SMT parameters
[b]Parameters measured directly (by SMT and smFISH) and input into the transcription model
[c]Parameters obtained by fitting the smFISH data to the transcription model while varying only k_{tx} and t_{prod}
[d]Parameter values found by fitting the smFISH data to the transcription model by varying S_{eq}, k_{on}, k_{tx}, and t_{prod}

We input into the model the parameters for the gene "OFF" (k_{off}) and "ON" rate (k_{on} and S_{eq}) and the mRNA degradation rate obtained by measuring a smFISH time course in fixed cells (Figure S5D). Many sets of the other parameters were then simulated to generate mRNA distributions that were compared to the smFISH distributions. The final parameter values were then found by taking the average of the 1,000 parameter sets that generated distributions most similar to the experimental data (Figure 5C). As we always fix the binding k_{off} to the value measured by SMT to constrain the model, it is not possible for us to directly test the assumption that the "OFF" rate is accurately described by k_{off}. However, we validated the assumption that the "ON" rate is accurately described by k_{on} by letting all the parameters except k_{off} vary in our fitting procedure for smFISH data. In this case the fitting procedure returns a value of k_{on} that is very similar to the value calculated from SMT data and the fraction of non-active cells estimated from smFISH data (Table 1). If, alternatively, the switch to the "ON" state would be regulated by several factors and the binding of Ace1p alone would be insufficient to switch the gene into the "ON" state, we would expect to see a different value of k_{on} returned, either because the "ON" rate of the gene is not related to the TF binding "on" rate or because the "OFF" rate is not related to the TF "off" rate, and therefore the "ON" rate needed to change to make the ratio of k_{on}/k_{off} correct. Thus, binding of Ace1p appears to be the rate-limiting step for *CUP1* to turn both "ON" and "OFF," which is consistent with the assumption that the switch to the "ON" state requires only binding of Ace1p.

We then used the primary parameters from the model to obtain the characteristics of the transcriptional bursts (Table 1 and Figure 5D). Remarkably, the estimates for polymerase initiation (k_{tx}) and elongation (t_{prod}) remain nearly the same for Rsc2$^+$ and Rsc2$^-$ cells. The production time is 70.2 ± 21.0 s for Rsc2$^+$ and 80.9 ± 43.5 for Rsc2$^-$ (p value 0.68; z test), and the initiation rate is 0.18 ± 0.03 mRNA/s for Rsc2$^+$ and 0.24 ± 0.08 mRNA/s for Rsc2$^-$ (p value 0.17, z test). Thus, RSC acts at the preinitiation step and does not affect the subsequent stages of transcription. Therefore, we conclude that RSC modulates transcription solely by modulating TF binding. Rsc2p halves the burst duration from 5.22 ± 0.82 s to 2.18 ± 0.33 s and increases the burst frequency by roughly a factor of three, from 0.04 ± 0.01 s^{-1} to 0.12 ± 0.03 s^{-1}. Due to the constant initiation rate and decreasing burst duration, the amplitude of each burst also decreases from 1.28 ± 0.47 mRNA in Rsc2$^-$ to 0.39 ± 0.09 mRNA in

Figure 4. RSC Affects the "on" Rate of Ace1p and the Availability of RE at the *CUP1* Promoter

(A) Diagram of the targeted integration of *CUP1* reporter into *CUP1* array (not to scale). The cassette contains a scrambled sequence derived from mammalian gene (scr. mam) and eight copies of the phage MS2 binding site that may be transcribed in a single transcript, but cannot be translated. *LEU2* is used as a selective marker for integration. Positions of the primers used to amplify the cassette are marked in magenta (T1010) and cyan (T1004).

(B) Maximum intensity projections of z stack of a diploid cell containing the *CUP1* reporter inserted into one of the two *CUP1* arrays. TAMRA (red), reporter mRNA stained by smFISH probes; Ace1p-3xGFP (green), *CUP1* locus; DAPI (blue), nucleus. Overlays: *CUP1* reporter mRNA colocalizes with only one of the two *CUP1* transcription sites (arrowhead). Scale bar, 2 μm.

(C) Population of cells with *CUP1* reporter: transcribing (yellow circles), i.e., containing > 3 molecules of mature mRNA, and not transcribing (blue circles). Overlays of DAPI (green) and *CUP1* reporter mRNA (red) are shown. Maximal intensity projections of the z stacks of the images of the cells treated by 100 μM Cu^{2+} for *CUP1* activation and 1 mM auxin for Rsc2 depletion and control cells of YTK1649 are presented. Original 15-bit images were scaled in Metamorph with linear LUT with the same range for brightness and contrast. Scale bar, 2 μm.

(D) Counts of mature mRNA in control cells not activated by Cu^{2+} (upper panel, black bars) are fit to Poisson distribution with mean 0.46. The same Poisson distribution (mean 0.46) can be used to fit the initial points of the distribution of mature mRNA in cells activated by Cu^{2+}, both Rsc2$^+$ and Rsc2p$^-$, if it is first scaled by a constant factor, α.

(E) Histograms of mature mRNA per cell. The population of non-active cells (blue) was obtained by fitting the histogram cut-off at 3 mRNA/cell to a scaled Poisson distribution with a fixed mean of 0.46 mRNA/cell estimated from the non-activated control. The scaling parameter in the fit is used to define the fraction of non-active cells, as represented in blue fonts.

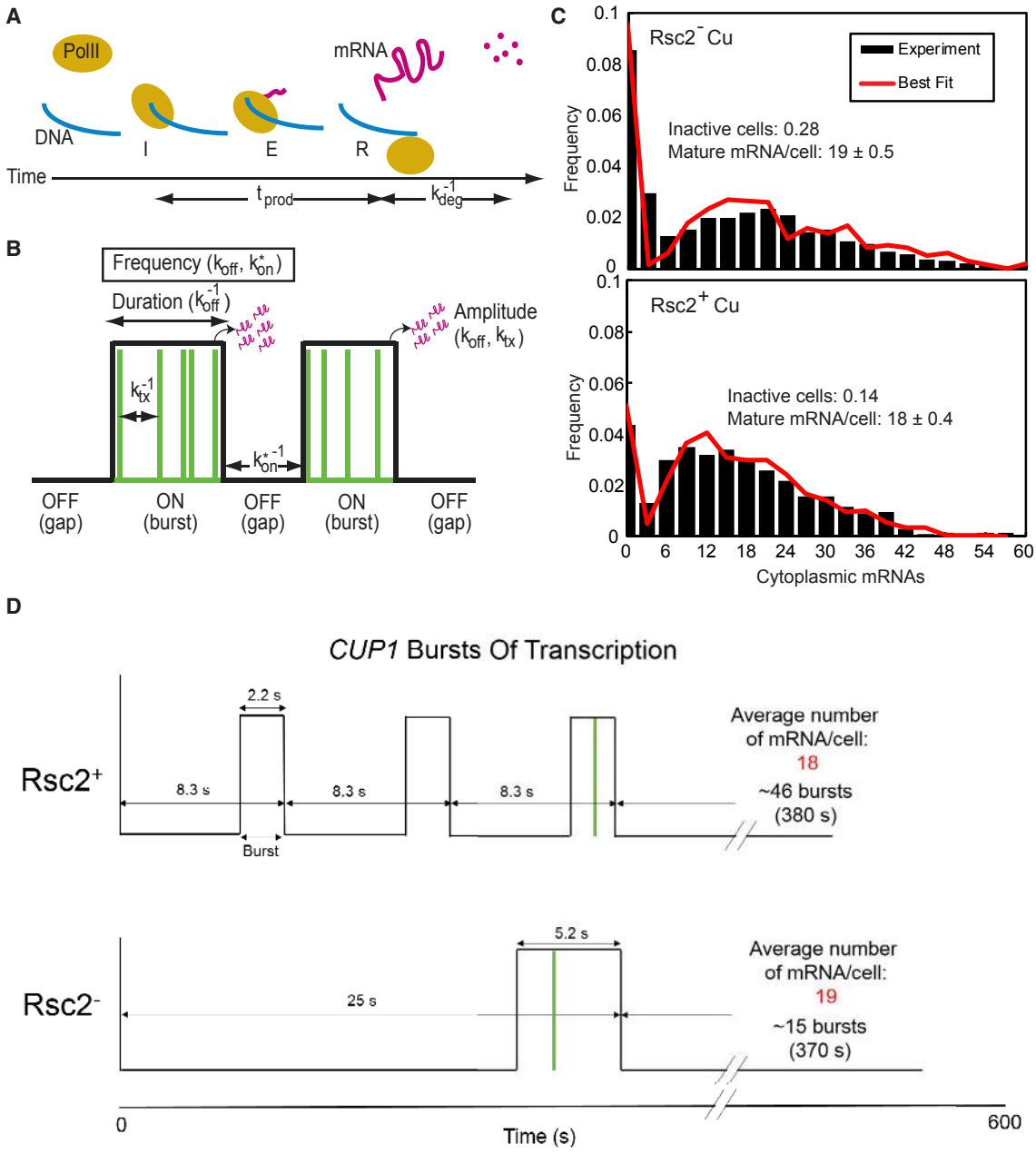

Figure 5. RSC Acts at Preinitiation Stage

(A) The production rate, t_{prod}, for a single mRNA (pink line) is defined here as the time from initiation "I" through elongation "E" to release "R" of the mature mRNA. Mature mRNA then degrades with an average lifetime of k_{deg}^{-1}.

(B) The gene switches between an ON state and an OFF state (black line). During a burst, transcription is initiated at random (green lines). The rate parameters characterize the frequency of bursts (k^*_{on} and k_{off}), duration of a burst (k_{off}), and the amplitude of a burst (k_{tx} and k_{off}).

(C) Histogram and bursting gene expression fits (red) of mature mRNA in Rsc2$^-$ and Rsc2$^+$. Fit lines were obtained by simulating the model with the average values of 1,000 parameter sets that fit the data well.

(D) Schematics of *CUP1* burst dynamics in Rsc2$^+$ and Rsc2$^-$ cells based on parameters estimated by the gene busting model of transcription.

Rsc2$^+$ (Table 1). More frequent bursts in Rsc2$^+$ are canceled out by decreased duration and amplitude, and thus the same mean value for mature mRNA per active cell is observed in Rsc2$^+$ and Rsc2$^-$ cells.

The Role of RSC Chromatin Remodeler Complex in the Nucleosomal Mobility at *CUP1*

Interestingly, based on predictions of the random gene bursting model, transcription from an individual *CUP1* gene occurs as a

A Rsc2p SMT

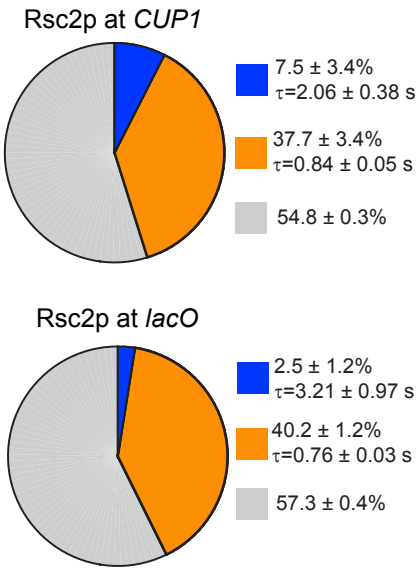

	CUP1	*lacO*
Total tracks	2051	1215
Bound particles	13729	6167
Total particles	30421	14686

B MNase-seq of *CUP1* locus

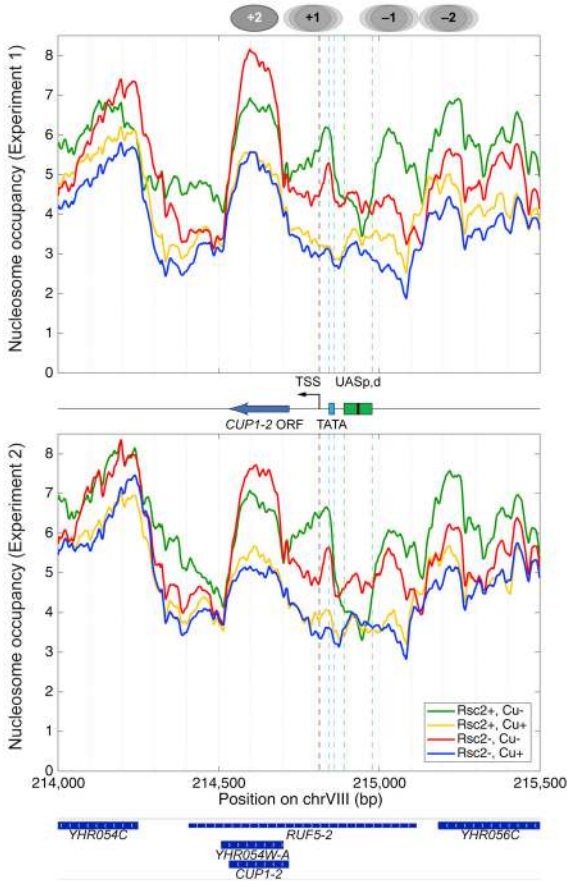

C Dynamic exchange of Ace1p and RSC complex at activated *CUP1* promoter

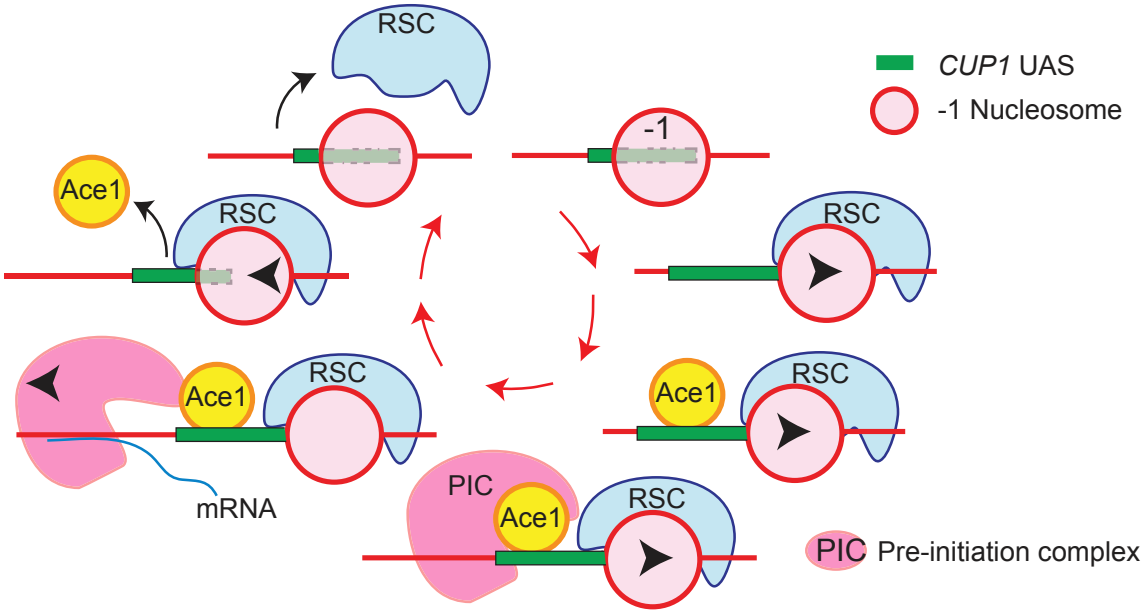

(legend on next page)

batch of very short and fast bursts. This behavior may be explained by cycles of rapid remodeling events that facilitate the cycles of productive TF binding, and thus we decided to quantify the binding of RSC to promoters of *CUP1*. We compared by SMT Rsc2p-HaloTag-JF_{646} binding at both *CUP1* and *lacO* (Figure 6A). Consistent with the fact that RSC can bind to chromatin at multiple sites across the genome, we observed a biexponential distribution of residence times for Rsc2p at both *CUP1* and *lacO*. However, a 3× increase in the slow-bound fraction of Rsc2p at the activated *CUP1* locus compared to *lacO* (7.5% ± 3.4% versus 2.5% ± 1.2%; p = 0.007) suggests that more specific binding of Rsc2p occurs at the transcriptionally active *CUP1*. The residence time of Rsc2p decreases from 3.2 s to 2.1 s. Therefore, as both Ace1p and RSC undergo fast cycling on active *CUP1* promoter, our data indicate that preinitiation at *CUP1* is dependent on short repetitive remodeling events.

Mapping of nucleosomes by MNase-seq (Figure 6B) demonstrates that in cells not treated with Cu^{2+}, Rsc2p makes the chromatin structure of the *CUP1* region more regular and makes the distant upstream activating site (UAS) more accessible. Indeed, using ChIP we saw that Rsc2p is present at *CUP1* promoters even in the absence of activation (Figure 3A). After Cu^{2+} activation, *CUP1* chromatin structure becomes more irregular, which is consistent with heavy transcription, but it is almost unaffected by Rsc2p depletion. This is consistent with RT-qPCR data demonstrating transcription even in the absence of RSC. These data confirm that the remodeling activity of RSC at the activated *CUP1* must occur rapidly and cyclically, leading to rapid back and forth movements of the nucleosomes, so that the net effect on nucleosome occupancy in the population (the frequency with which the putative positions are occupied by nucleosomes) cannot be registered in MNase-seq experiments.

DISCUSSION

Binding of TFs to their REs has been quantified in real time by methods of *in vivo* biophysics. On the other hand, chromatin remodeling of activated promoters has mainly been studied by methods of molecular biology, which do not provide sufficient spatiotemporal resolution. Therefore, it is unknown on what timescale the chromatin remodeling occurs and how it relates to periodic binding of TFs. We adopted quantitative single-molecule approaches to investigate the molecular links between chromatin remodeling and the fast cycling of TFs on activated promoters.

Typically, SMT assays rely on averaging across multiple promoters, which may mask a substantial diversity. We focus on a specific site to reveal promoter-specific mechanisms of regulation. We discovered an alternative mechanism of regulation for Ace1p occupancy by RSC via an increase in molecular binding rate and in the availability of REs. Significantly, improvement of TF search by remodeling is totally sufficient to explain observed effects of the remodeler RSC on the transcription of *CUP1*, without requiring any modification to other transcriptional parameters such as polymerase initiation or elongation rates.

How Can Remodelers Affect the Search and Residence Time of the TF?

We found that RSC improves the search of Ace1p for specific REs in two ways: first, by increasing the availability of REs from 1.1 to 1.5 sites out of four, and second, by improving k_{on}. RSC may improve k_{on} by providing larger stretches of nucleosome-free DNA, which may (1) lead to a change in the size of the search target and (2) facilitate search by allowing the non-specifically bound TF to slide along the DNA to its RE (Mirny et al., 2009). In addition, clustering of accessible REs in the same promoter improves the probability that a TF will find at least one. Of course, we cannot exclude the possibility that the improvement in k_{on} is caused by a direct interaction between RSC and Ace1p. However, as the search of Ace1p for an RE depends on the RE availability as much as on k_{on}, RSC must affect the search at least partially, or completely by chromatin remodeling. We also observe that RSC reduces the residence time of Ace1p on RE, most likely by remodeling. This idea is supported by published *in vitro* experiments demonstrating displacement of a TF by a chromatin remodeler (Li et al., 2015; Nagaich et al., 2004).

How Does Modified Binding of TF Affect the Transcription?

We estimated the transcription parameters in RSC^+ and RSC^- cells by modeling mRNA output of individual cells measured by smFISH. Our model predicts a batch of ~50 frequent short bursts of transcription for *CUP1*. Note that estimates of the burst amplitude indicate that only one of the three bursts in $Rsc2^+$ cells leads to the production of mature mRNA. Modulation of TF binding effected by RSC leads to changes in burst frequency and duration but doesn't affect the transcription initiation rate and transcript production rate.

Surprisingly, although RSC depletion increases copper sensitivity (Figure 3C), the net change in transcription is small. Taking into the account the non-activated cells present in the population, the overall output from $Rsc2^-$ cells is reduced only by ~2%. More efficient production of mature mRNA in $Rsc2p^-$ cells, which correlates with longer residence time of Ace1p, partially compensates for the less frequent bursts. In other systems an increase in burst frequency leads to an efficient increase in transcription output (Larson et al., 2013; Senecal et al., 2014).

Figure 6. The Role of RSC Chromatin Complex in Nucleosomal Mobility at *CUP1*

(A) Single-molecule tracking of Rsc2p-HaloTag (JF646) at *CUP1* (YTK1635) and *pes4::lacO* (YTK1634). Charts and tables are as described in the caption to Figure 1C.

(B) Nucleosomal occupancy at *CUP1*. MNase-seq data for two biological replicate experiments are shown. *CUP1-2*, a single copy of *CUP1* within the array; UASp,d, proximal and distal upstream activating sequences, each containing two REs for Ace1p; ovals, approximate positions of nucleosomes before activation. Treatment conditions: $Rsc2^-$, $Rsc2^+$, with or without Cu activation.

(C) Proposed sequence of events at *CUP1* promoter for an individual molecule of Ace1p: a molecule of RSC recruited to *CUP1* mobilizes the −1 nucleosome, promoting binding of Ace1p; next, a bound molecule of Ace1p recruits the preinitiation complex (PIC); next, transcription starts, and PIC is disassembled; next, RSC moves the −1 nucleosome in opposite direction, promoting eviction of Ace1p molecule.

What is the advantage of more frequent bursts, if they do not lead to a significant improvement in the transcription output per cell? RSC makes more cells competent for transcription, and RSC activity reduces the transcriptional noise of the system, as can be demonstrated by the reduction in Fano factor from 8.8 in active $Rsc2^-$ cells to 6.1 in $Rsc2^+$ cells. Physiologically, this translates into a more uniform response of the population to a heavy metal stress. Notably, data for HIV expression indicate that more frequent bursts may increase the efficiency of the response to an external stimulus and that the difference in chromatin state may affect the transcription noise (Wong et al., 2018).

Do the Rapid and Frequent Bursts Depend on Rapid and Frequent Remodeling?

Interestingly, we show by MNase-seq that RSC has a moderate effect on nucleosomal architecture of *CUP1* promoter only in inactive cells. No effect on nucleosomal occupancy and/or changes in the length of nucleosome-depleted regions can be observed in activated cells. However, MNase-seq demonstrates a shift to a fluid chromatin state in activated cells (Figure 6B). Thus, remodeling events initiated by RSC may be short and transient. Indeed, as observed by SMT, RSC is rapidly cycling on *CUP1*, on the timescale comparable to that of Ace1p (Figure 6A). Repetitive rapid bursts of *CUP1* transcription (Figure 5D) point to rapid cycles of chromatin remodeling and TF binding. We propose the following model for the correlation of TF cycling, remodeling, and transcription (Figure 6C). RSC affects Ace1p binding by increasing the rate at which nucleosomes shift from one position to another. Removal of the non-essential Rsc2p subunit of RSC slows down the cycling of Ace1p by decreasing the nucleosomal mobilization rate. The cycle starts when an individual RSC molecule, binding to the UAS of *CUP1*, moves the −1 nucleosome from the partially obstructed RE and facilitates binding of an Ace1p molecule to the UAS. Binding of Ace1p switches the gene to the "ON" state. Ace1p recruits the components of the PIC and facilitates transcription. The next steps of the transcription process are not dependent on Ace1p. RSC removes Ace1p from the UAS by moving the −1 nucleosome into the UAS, and the gene switches to the "OFF" state.

Relevance of the Interdependent Dynamics of RSC and Ace1p at *CUP1* Promoter to Mammalian Genes

The *CUP1* promoter is regulated only by two mutually exclusive pathways (heavy metal stress or heat shock response) controlled by either Ace1p or Hsf1p and contains only four REs for Ace1p and two for Hsf1p. Due to the limited number of interacting factors and REs, this is an ideal system for modeling dynamics of TFs and chromatin remodelers. Mammalian promoters and enhancers quite often contain multiple REs for multiple TFs and may be regulated simultaneously by multiple pathways, which makes similar analysis much more complicated. However, we expect that on the molecular level this multi-component regulation may be dissected into simple dynamic interactions analogous to those described in this paper. Specifically, we expect that regulation by search improvement may be important for those mammalian promoters that have to respond quickly and uniformly to environmental stress and for which it is not critical to quickly turn off the gene by reducing residence time of the TF. Moreover, data from other groups indicate that the same mechanisms may also work for enhancers of multicellular eukaryotes, such as those regulated by the mammalian glucocorticoid receptor (GR). Hoffman et al., 2018 demonstrated by ChIP-seq the interdependent facilitation of RE occupancy by GR and the chromatin remodeler BRG1: binding of BRG1 is required to recruit GR, and GR recruits BRG1, which further improves GR binding. We expect the same at *CUP1*, as we observe that the RSC complex is bound at *CUP1* in inactive cells, and after activation, when Ace1p binds, RSC is enriched at *CUP1* (Figure 3A). Further support for the interdependent dynamics of TFs and chromatin remodelers may be derived from the cycles of remodeling, TF binding, and TF release that were observed *in vitro* for the reconstructed mouse mammary tumor virus (MMTV) enhancer array (Nagaich et al., 2004). In this system SWI/SNF chromatin remodeling complex facilitated not only binding to RE, but also the release of the glucocorticoid receptor (GR) from its RE on the MMTV promoter. Notably, the frequency of the binding-release cycle was dependent on the ratio of GR to SWI/SNF in the reaction mix, thus on the efficiency of remodeling.

In sum, we demonstrate a link between chromatin remodeling and transient binding of transcription factors to specific sites in promoters. Since nucleosome displacement by remodelers is widespread in all eukaryotes, we expect that transcription from many other genes will be similarly regulated by remodeler action.

STAR★METHODS

Detailed methods are provided in the online version of this paper and include the following:

- KEY RESOURCES TABLE
- CONTACT FOR REAGENT AND RESOURCE SHARING
- EXPERIMENTAL MODEL AND SUBJECT DETAILS
  - Yeast strains and plasmids
  - Media and growth conditions
- METHOD DETAILS
  - Chromatin immunoprecipitation (ChIP)
  - Quantitative RT-PCR (RT-qPCR)
  - Protein concentration by western blots
  - Quantification of Ace1p-GFP
  - Custom-built Microscope for SMT
  - SMT: staining, imaging, and quantification
  - smFISH: staining, imaging, and quantification
  - mRNA degradation rate
  - *CUP1* nucleosome occupancy by MNase-seq
- QUANTIFICATION AND STATISTICAL ANALYSIS
  - Relationship between SMT parameters
  - Estimating fraction of non-active cells
  - Estimation of $S_{Equation}$ and k_{on}
  - Monte Carlo Simulations of TF binding
  - Curve-fitting of mature transcript distributions
- DATA AND SOFTWARE AVAILABILITY

SUPPLEMENTAL INFORMATION

Supplemental Information includes six figures, three tables, and two videos and can be found with this article online at https://doi.org/10.1016/j.molcel.2018.09.009.

ACKNOWLEDGMENTS

This work was supported by Intramural Research Program of National Institutes of Health (NCI, NICHD, CCR). Funding for the open access charge comes from the Intramural Research Program of NIH. We thank Brian English and Tatsuya Morisaki for their advice in the design of the custom microscope; NHLBI Core Facility for paired-end sequencing; Florian Mueller for the advice on using FISH-quant; Brad Cairns and Helle Ulrich for the plasmids; Luke Lavis for the JF dyes; and David Auble, Yuri Chernoff, and Matthew Ferguson for the critical reading of the manuscript. This study utilized the high-performance computational capabilities of the Biowulf Linux cluster at the National Institutes of Health.

AUTHOR CONTRIBUTIONS

G.D.M. constructed strains and plasmids and carried out and analyzed most of the experiments; D.A.B. conducted computer simulations; D.J.C. designed and P.R.E. and R.V.C. carried out and quantified MNase-seq experiments. T.S.K. provided overall experimental design and J.G.M. provided biophysical guidelines. T.S.K., J.G.M., D.A.B., and G.D.M. wrote the manuscript.

DECLARATION OF INTERESTS

The authors declare no competing interests.

Received: May 21, 2018
Revised: August 8, 2018
Accepted: September 7, 2018
Published: October 11, 2018

SUPPORTING CITATIONS

The following references appear in the Supplemental Information: Shen et al. (2002).

REFERENCES

Ball, D.A., Mehta, G.D., Salomon-Kent, R., Mazza, D., Morisaki, T., Mueller, F., McNally, J.G., and Karpova, T.S. (2016). Single molecule tracking of Ace1p in Saccharomyces cerevisiae defines a characteristic residence time for non-specific interactions of transcription factors with chromatin. Nucleic Acids Res. *44*, e160.

Bowman, G.D., and McKnight, J.N. (2017). Sequence-specific targeting of chromatin remodelers organizes precisely positioned nucleosomes throughout the genome. BioEssays *39*, 1–8.

Buchman, C., Skroch, P., Dixon, W., Tullius, T.D., and Karin, M. (1990). A single amino acid change in CUP2 alters its mode of DNA binding. Mol. Cell. Biol. *10*, 4778–4787.

Cairns, B.R., Schlichter, A., Erdjument-Bromage, H., Tempst, P., Kornberg, R.D., and Winston, F. (1999). Two functionally distinct forms of the RSC nucleosome-remodeling complex, containing essential AT hook, BAH, and bromodomains. Mol. Cell *4*, 715–723.

Chereji, R.V., Ocampo, J., and Clark, D.J. (2017). MNase-Sensitive Complexes in Yeast: Nucleosomes and Non-histone Barriers. Mol. Cell *65*, 565–577.e3.

Clauß, K., Popp, A.P., Schulze, L., Hettich, J., Reisser, M., Escoter Torres, L., Uhlenhaut, N.H., and Gebhardt, J.C.M. (2017). DNA residence time is a regulatory factor of transcription repression. Nucleic Acids Res. *45*, 11121–11130.

Cole, H.A., Howard, B.H., and Clark, D.J. (2012). Genome-wide mapping of nucleosomes in yeast using paired-end sequencing. Methods Enzymol. *513*, 145–168.

Das, R., Cairo, C.W., and Coombs, D. (2009). A hidden Markov model for single particle tracks quantifies dynamic interactions between LFA-1 and the actin cytoskeleton. PLoS Comput. Biol. *5*, e1000556.

Edelstein, A.D., Tsuchida, M.A., Amodaj, N., Pinkard, H., Vale, R.D., and Stuurman, N. (2014). Advanced methods of microscope control using μManager software. J. Biol. Methods *1*, e10.

English, B.P., and Singer, R.H. (2015). A three-camera imaging microscope for high-speed single-molecule tracking and super-resolution imaging in living cells. Proc SPIE Int Soc Opt Eng *9550*, 955008.

Fürst, P., Hu, S., Hackett, R., and Hamer, D. (1988). Copper activates metallothionein gene transcription by altering the conformation of a specific DNA binding protein. Cell *55*, 705–717.

Gillespie, D.T. (1977). Exact stochastic simulation of coupled chemical reactions. J. Phys. Chem. *81*, 2340–2361.

Grimm, J.B., English, B.P., Chen, J., Slaughter, J.P., Zhang, Z., Revyakin, A., Patel, R., Macklin, J.J., Normanno, D., Singer, R.H., et al. (2015). A general method to improve fluorophores for live-cell and single-molecule microscopy. Nat. Methods *12*, 244–250, 3, 250.

Gross, C., Kelleher, M., Iyer, V.R., Brown, P.O., and Winge, D.R. (2000). Identification of the copper regulon in Saccharomyces cerevisiae by DNA microarrays. J. Biol. Chem. *275*, 32310–32316.

Güldener, U., Heck, S., Fielder, T., Beinhauer, J., and Hegemann, J.H. (1996). A new efficient gene disruption cassette for repeated use in budding yeast. Nucleic Acids Res. *24*, 2519–2524.

Hoffman, J.A., Trotter, K.W., Ward, J.M., and Archer, T.K. (2018). BRG1 governs glucocorticoid receptor interactions with chromatin and pioneer factors across the genome. eLife *7*, e35073.

Hoopes, B.C., LeBlanc, J.F., and Hawley, D.K. (1992). Kinetic analysis of yeast TFIID-TATA box complex formation suggests a multi-step pathway. J. Biol. Chem. *267*, 11539–11547.

Izeddin, I., Récamier, V., Bosanac, L., Cissé, I.I., Boudarene, L., Dugast-Darzacq, C., Proux, F., Bénichou, O., Voituriez, R., Bensaude, O., et al. (2014). Single-molecule tracking in live cells reveals distinct target-search strategies of transcription factors in the nucleus. eLife *3*.

Janke, C., Magiera, M.M., Rathfelder, N., Taxis, C., Reber, S., Maekawa, H., Moreno-Borchart, A., Doenges, G., Schwob, E., Schiebel, E., and Knop, M. (2004). A versatile toolbox for PCR-based tagging of yeast genes: new fluorescent proteins, more markers and promoter substitution cassettes. Yeast *21*, 947–962.

Karpova, T.S., Chen, T.Y., Sprague, B.L., and McNally, J.G. (2004). Dynamic interactions of a transcription factor with DNA are accelerated by a chromatin remodeller. EMBO Rep. *5*, 1064–1070.

Karpova, T.S., Kim, M.J., Spriet, C., Nalley, K., Stasevich, T.J., Kherrouche, Z., Heliot, L., and McNally, J.G. (2008). Concurrent fast and slow cycling of a transcriptional activator at an endogenous promoter. Science *319*, 466–469.

Kim, J.G., Takeda, Y., Matthews, B.W., and Anderson, W.F. (1987). Kinetic studies on Cro repressor-operator DNA interaction. J. Mol. Biol. *196*, 149–158.

Kleinschmidt, C., Tovar, K., Hillen, W., and Porschke, D. (1988). Dynamics of repressor-operator recognition: the Tn10-encoded tetracycline resistance control. Biochemistry *27*, 1094–1104.

Larson, D.R., Fritzsch, C., Sun, L., Meng, X., Lawrence, D.S., and Singer, R.H. (2013). Direct observation of frequency modulated transcription in single cells using light activation. eLife *2*, e00750.

Li, M., Hada, A., Sen, P., Olufemi, L., Hall, M.A., Smith, B.Y., Forth, S., McKnight, J.N., Patel, A., Bowman, G.D., et al. (2015). Dynamic regulation of transcription factors by nucleosome remodeling. eLife *4*, https://doi.org/10.7554/eLife.06249.

Liao, Y., Schroeder, J.W., Gao, B., Simmons, L.A., and Biteen, J.S. (2015). Single-molecule motions and interactions in live cells reveal target search dynamics in mismatch repair. Proc. Natl. Acad. Sci. USA *112*, E6898–E6906.

Lickwar, C.R., Mueller, F., Hanlon, S.E., McNally, J.G., and Lieb, J.D. (2012). Genome-wide protein-DNA binding dynamics suggest a molecular clutch for transcription factor function. Nature *484*, 251–255.

Loffreda, A., Jacchetti, E., Antunes, S., Rainone, P., Daniele, T., Morisaki, T., Bianchi, M.E., Tacchetti, C., and Mazza, D. (2017). Live-cell p53 single-molecule binding is modulated by C-terminal acetylation and correlates with transcriptional activity. Nat. Commun. *8*, 313.

Longtine, M.S., McKenzie, A., 3rd, Demarini, D.J., Shah, N.G., Wach, A., Brachat, A., Philippsen, P., and Pringle, J.R. (1998). Additional modules for

versatile and economical PCR-based gene deletion and modification in Saccharomyces cerevisiae. Yeast *14*, 953–961.

Mazza, D., Abernathy, A., Golob, N., Morisaki, T., and McNally, J.G. (2012). A benchmark for chromatin binding measurements in live cells. Nucleic Acids Res. *40*, e119.

Mazza, D., Ganguly, S., and McNally, J.G. (2013). Monitoring dynamic binding of chromatin proteins in vivo by single-molecule tracking. Methods Mol. Biol. *1042*, 117–137.

Mehta, G.D., Agarwal, M., and Ghosh, S.K. (2014). Functional characterization of kinetochore protein, Ctf19 in meiosis I: an implication of differential impact of Ctf19 on the assembly of mitotic and meiotic kinetochores in Saccharomyces cerevisiae. Mol. Microbiol. *91*, 1179–1199.

Mirny, L., Slutsky, M., Wunderlich, Z., Tafvizi, A., Leith, J., and Kosmrlj, A. (2009). How a protein searches for its site on DNA: the mechanism of facilitated diffusion. J. Phys. A Math. Theor. *42*, 1–23.

Morawska, M., and Ulrich, H.D. (2013). An expanded tool kit for the auxin-inducible degron system in budding yeast. Yeast *30*, 341–351.

Morisaki, T., Müller, W.G., Golob, N., Mazza, D., and McNally, J.G. (2014). Single-molecule analysis of transcription factor binding at transcription sites in live cells. Nat. Commun. *5*, 4456.

Morisaki, T., Lyon, K., DeLuca, K.F., DeLuca, J.G., English, B.P., Zhang, Z., Lavis, L.D., Grimm, J.B., Viswanathan, S., Looger, L.L., et al. (2016). Real-time quantification of single RNA translation dynamics in living cells. Science *352*, 1425–1429.

Mueller, F., Senecal, A., Tantale, K., Marie-Nelly, H., Ly, N., Collin, O., Basyuk, E., Bertrand, E., Darzacq, X., and Zimmer, C. (2013). FISH-quant: automatic counting of transcripts in 3D FISH images. Nat. Methods *10*, 277–278.

Nagaich, A.K., Walker, D.A., Wolford, R., and Hager, G.L. (2004). Rapid periodic binding and displacement of the glucocorticoid receptor during chromatin remodeling. Mol. Cell *14*, 163–174.

Nishimura, K., Fukagawa, T., Takisawa, H., Kakimoto, T., and Kanemaki, M. (2009). An auxin-based degron system for the rapid depletion of proteins in nonplant cells. Nat. Methods *6*, 917–922.

Paakinaho, V., Presman, D.M., Ball, D.A., Johnson, T.A., Schiltz, R.L., Levitt, P., Mazza, D., Morisaki, T., Karpova, T.S., and Hager, G.L. (2017). Single-molecule analysis of steroid receptor and cofactor action in living cells. Nat. Commun. *8*, 15896.

Peña, M.M., Koch, K.A., and Thiele, D.J. (1998). Dynamic regulation of copper uptake and detoxification genes in Saccharomyces cerevisiae. Mol. Cell. Biol. *18*, 2514–2523.

Persson, F., Lindén, M., Unoson, C., and Elf, J. (2013). Extracting intracellular diffusive states and transition rates from single-molecule tracking data. Nat. Methods *10*, 265–269.

Poorey, K., Viswanathan, R., Carver, M.N., Karpova, T.S., Cirimotich, S.M., McNally, J.G., Bekiranov, S., and Auble, D.T. (2013). Measuring chromatin interaction dynamics on the second time scale at single-copy genes. Science *342*, 369–372.

Presman, D.M., Ball, D.A., Paakinaho, V., Grimm, J.B., Lavis, L.D., Karpova, T.S., and Hager, G.L. (2017). Quantifying transcription factor binding dynamics at the single-molecule level in live cells. Methods *123*, 76–88.

Raj, A., and Tyagi, S. (2010). Detection of individual endogenous RNA transcripts in situ using multiple singly labeled probes. Methods Enzymol. *472*, 365–386.

Raj, A., Peskin, C.S., Tranchina, D., Vargas, D.Y., and Tyagi, S. (2006). Stochastic mRNA synthesis in mammalian cells. PLoS Biol. *4*, e309.

Riggs, A.D., Bourgeois, S., and Cohn, M. (1970). The lac repressor-operator interaction. 3. Kinetic studies. J. Mol. Biol. *53*, 401–417.

Rohner, S., Gasser, S.M., and Meister, P. (2008). Modules for cloning-free chromatin tagging in Saccharomyces cerevisiae. Yeast *25*, 235–239.

Senecal, A., Munsky, B., Proux, F., Ly, N., Braye, F.E., Zimmer, C., Mueller, F., and Darzacq, X. (2014). Transcription factors modulate c-Fos transcriptional bursts. Cell Rep. *8*, 75–83.

Shen, C.H., Leblanc, B.P., Alfieri, J.A., and Clark, D.J. (2001). Remodeling of yeast CUP1 chromatin involves activator-dependent repositioning of nucleosomes over the entire gene and flanking sequences. Mol. Cell. Biol. *21*, 534–547.

Shen, C.H., Leblanc, B.P., Neal, C., Akhavan, R., and Clark, D.J. (2002). Targeted histone acetylation at the yeast CUP1 promoter requires the transcriptional activator, the TATA boxes, and the putative histone acetylase encoded by SPT10. Mol. Cell. Biol. *22*, 6406–6416.

Stavreva, D.A., Müller, W.G., Hager, G.L., Smith, C.L., and McNally, J.G. (2004). Rapid glucocorticoid receptor exchange at a promoter is coupled to transcription and regulated by chaperones and proteasomes. Mol. Cell. Biol. *24*, 2682–2697.

Tokunaga, M., Imamoto, N., and Sakata-Sogawa, K. (2008). Highly inclined thin illumination enables clear single-molecule imaging in cells. Nat. Methods *5*, 159–161.

Tsabar, M., Haase, J., Harrison, B., Snider, C.E., Eldridge, B., Kaminsky, L., Hine, R.M., Haber, J.E., and Bloom, K. (2016). A Cohesin-Based Partitioning Mechanism Revealed upon Transcriptional Inactivation of Centromere. PLoS Genet. *12*, e1006021.

Van Royen, M.E., van Cappellen, W.A., Geverts, B., Schmidt, T., Houtsmuller, A.B., and Schaaf, M.J. (2014). Androgen receptor complexes probe DNA for recognition sequences by short random interactions. J. Cell Sci. *127*, 1406–1416.

Voss, T.C., and Hager, G.L. (2014). Dynamic regulation of transcriptional states by chromatin and transcription factors. Nat. Rev. Genet. *15*, 69–81.

Wong, V.C., Bass, V.L., Bullock, M.E., Chavali, A.K., Lee, R.E.C., Mothes, W., Gaudet, S., and Miller-Jensen, K. (2018). NF-κB-Chromatin Interactions Drive Diverse Phenotypes by Modulating Transcriptional Noise. Cell Rep. *22*, 585–599.

Zenklusen, D., Larson, D.R., and Singer, R.H. (2008). Single-RNA counting reveals alternative modes of gene expression in yeast. Nat. Struct. Mol. Biol. *15*, 1263–1271.

Zhao, Y., Strope, P.K., Kozmin, S.G., McCusker, J.H., Dietrich, F.S., Kokoska, R.J., and Petes, T.D. (2014). Structures of naturally evolved CUP1 tandem arrays in yeast indicate that these arrays are generated by unequal nonhomologous recombination. G3 (Bethesda) *4*, 2259–2269.

STAR★METHODS

KEY RESOURCES TABLE

REAGENT or RESOURCE	SOURCE	IDENTIFIER
Antibodies		
Goat polyclonal Anti-Myc tag Antibody (ChIP grade)	Abcam	ab9132; RRID:AB_307033
Mouse anti-HA tag antibody (clone 12CA5)	Roche	11583816001; RRID:AB_514505
Mouse anti-c-Myc tag antibody (clone 9E10)	Roche	11667149001; RRID:AB_390912
Rabbit polyclonal Anti-HaloTag antibodies	Promega	G9281; RRID:AB_713650
Rabbit anti-Tub2 antibody (crude serum)	Munira Basrai	N/A
AffiniPure goat anti-mouse IgG (H+L), HRP-conjugated	Jackson	115-035-003; RRID:AB_10015289
AffiniPure goat anti-rabbit IgG (H+L), HRP-conjugated	Jackson	111-035-144; RRID:AB_2307391
Bacterial and Virus Strains		
Full list of Bacterial strains is presented in Table S2.		
Chemicals, Peptides, and Recombinant Proteins		
Indole-3-Acetic Acid	Sigma	I5148
JF646	Grimm et al., 2015	N/A
Yeast Nitrogen Base with Ammonium sulfate	MP Biomedicals	4027-522
CSM	MP Biomedicals	4500-012
CSM-HIS	MP Biomedicals	4510-312
CSM-URA	MP Biomedicals	4511-212
CSM-LEU	MP Biomedicals	4510-512
DOBA	MP Biomedicals	4026-022
SeaKem GTG Agarose	Lonza	50070
Vectashield Antifade Mounting Medium with DAPI	Vector Laboratories	H-1200
Ribonucleoside Vanadyl Complexes 200 mM	Sigma	R3380
Glucose oxidase from *Aspergillus niger*	Sigma	G0543
Catalase from bovine liver	Sigma	C3155
Poly-L-lysine solution (0.1%)	Sigma	P8920
Critical Commercial Assays		
iQ SYBR Green Supermix	Bio-Rad	170-8882
PreCR Repair Mix	NEB	M0309
NEBNext Ultra DNA Library Prep Kit for illumina	NEB	E7370
NEB Next Multiplex Oligos for illumine	NEB	E7335
GFP-TRAP_MA	ChromoTek	gtma-20
Magna ChIP Protein A+G Magnetic Beads	Millipore	16-663
cOmplete EDTA-free protease inhibitor cocktail tablets	Roche	11873580001
Wizard SV Gel and PCR clean up system	Promega	A9282
2x Laemmli Sample Buffer	Bio-Rad	161-0737
4-20% Mini-Protean TGX Precast Gels, 10 wells	Bio-Rad	456-1094
Immun-Blot PVDF Membranes for protein Blotting	Bio-Rad	162-0177
Amersham ECL Prime Western Blotting Detection Reagent	GE Healthcare	RPN2232
iScript cDNA Synthesis Kit	Bio-Rad	1708891
Deposited Data		
MNase-seq data	NCBI Gene expression Omnibus	GEO: GSE112685
Original images of SMT, smFISH and western blot	Mendeley Data	https://doi.org/10.17632/hp9bwtnbgc.1

(*Continued on next page*)

Continued

REAGENT or RESOURCE	SOURCE	IDENTIFIER
Experimental Models: Organisms/Strains		
Full list of yeast strains is presented in Table S1.		
Oligonucleotides		
Full list of oligonucleotides is presented in Table S3.		
TAMRA-labeled custom-made Stellaris smFISH probes	LGC Biosearch Technologies	Figure S4 for probe sequences
Software and Algorithms		
TrackRecord (MatlabTrack_v5.4.4)	Ball et al., 2016	https://sourceforge.net/projects/single-molecule-tracking
FISH_Quant v3	Mueller et al., 2013	N/A
Gene Bursting Model for Transcription	Senecal et al., 2014	N/A
Monte Carlo simulations	Gillespie, 1977	N/A
MetaMorph	Molecular Devices	N/A
Fiji	NIH	https://fiji.sc/
R 3.4.0	Bell Laboratories	https://www.r-project.org/
Other		
LabTek II chambers, 2 wells, 1.5 mm cover glass	Nunc	155379

CONTACT FOR REAGENT AND RESOURCE SHARING

Further information and requests for resources and reagents should be directed to and will be fulfilled by the Lead Contact, Tatiana Karpova (karpovat@mail.nih.gov).

EXPERIMENTAL MODEL AND SUBJECT DETAILS

Yeast strains and plasmids

Saccharomyces cerevisiae strains used in this study were derived from the haploids BY4742, BY4741, and diploid BY4743 from the *Saccharomyces* deletion project, isogenic to S288C (Research Genetics/Invitrogen, Huntsville, AL) (see Table S1 for yeast strains and Table S2 for plasmids). Sequences and maps of plasmids are available upon request.

All strains carrying HaloTag fusions carried *pdr5*Δ to enhance HaloTag dye retention (Ball et al., 2016). Standard methods were used for yeast transformation (Güldener et al., 1996). For gene deletions and C-terminal tagging of proteins, appropriate PCR fragments (see Table S3 for primers) were introduced into the genome by homologous recombination (Janke et al., 2004; Longtine et al., 1998). All deletions and C-terminal tags were confirmed by either diagnostic PCR or observation of the localization of the appropriate fusions by fluorescent microscopy.

For *CUP1* locus visualization we used pTSK405 to amplify the 3x*GFP::URA3* cassette for endogenous tagging of *ACE1* in (YTK1390). For HaloTag fusions (YTK1391), we used pTSK561 (Ball et al., 2016) to amplify the *HaloTag::URA3* cassette. Both fusion proteins were expressed from wild-type *ACE1* promoter and thus were not overexpressed. No wild-type Ace1p was present in strains tested. Ace1p-3xGFP fusion and Ace1p-HaloTag fusion bind to *CUP1* (Figure S1A). Tagging of Ace1p did not affect the steady-state levels of *ACE1* mRNA (Figure S1B) and it did not affect either transcription of *CUP1* or resistance to copper (Figure S1C, S1D).

In YTK1528, *PES4* ORF was replaced with 256 copies of lacO by a two-step PCR based method (Rohner et al., 2008) using pUG73 (Euroscarf) and pSR7. To visualize *pes4::lacO, GFP-lacI* was integrated into *LYS2* as a *Ahd*I -*BspE*1 fragment of pLKL58Y (Tsabar et al., 2016).

For *RSC2* deletion, pUG27-borne *HIS5* cassette (Euroscarf) was amplified using primers T329 and T330 and transformed into YTK1396 and YTK1391.

For auxin-inducible degradation of Rsc2, the endogenous copy of *RSC2* was labeled as *RSC2-AID*-9MYC* or *RSC2-AID*-6HA* by amplifying the respective cassette from plasmid pHis-AID*-9Myc or pHyg-AID*-6HA (Morawska and Ulrich, 2013) using primers T882, T883. *pADH1-AFB2-CYCT1* was expressed constitutively from *Swa*I-digested pTSK559 integrated into *TRP1* locus; pTSK559 was constructed as follows. First, pTSK518 was synthesized by GenScript. Then *LEU2* was amplified from the yeast genome using T894 and T895 and cloned between *Xba*I-*Sac*I sites of pTSK518 to obtain pTSK554. Then *pADH1-AFB2-CYCT1* was amplified (using primers T896 and T897) from pRS303-pADH1-AFB2 (plasmid #99530, Addgene) and cloned into pTSK554 between *Sac*II-*Not*I to get pTSK559.

To visualize mRNA from a single copy of *CUP1* within the *CUP1* array, a *CUP1*-reporter was synthesized by GeneScript. It carried a scrambled non-translatable sequence based on the mammalian rat Glucocorticoid Receptor, to which 8 copies of MS2 binding sites were appended (Figure S4). The *CUP1*-reporter was amplified by PCR from pTSK588 using T1010 and T1004, and the PCR fragment was transformed into YTK1443 replacing the ORF of a single copy of *CUP1* within the array. It was expressed from the wild-type *CUP1* promoter (Figure 4A). We constructed plasmid pTSK588 by cloning the *CUP1*-reporter into pBSII SK (+) between *Xho*I-*Not*I sites and selection marker *LEU2* between NotI-SacI sites.

Media and growth conditions

Yeast cells were grown in complete synthetic media (CSM) with respective dropout amino acid mixture (MP Biomedicals). For all microscopy experiments, CSM (+respective dropout amino acid mixture) + 6.5 mg/mL Sodium Citrate was used. To monitor binding of Ace1p-3xGFP to the *CUP1* array, cells were treated by 100 μM $CuSO_4$. All experiments were performed at 30°C at 230 RPM.

For SMT, cultures grown overnight to saturation were diluted to 0.2 OD_{600} in 3 mL fresh media (in 14 mL polypropylene tubes, Cat no. 352059, Falcon, Maxico). Cells were grown for 4 hr. Cells were pelleted and resuspended in 1 mL of fresh media with 0.5 nM JF646. Cells were grown further for 30 min and harvested for imaging under the CSM+100 μM $CuSO_4$ containing agarose pads. For auxin-based depletion of Rsc2, Indole-3-acetic acid (IAA, Sigma, Cat no.: I5148) was added to the culture media at 1 mM concentration 4 hr before harvesting for the complete degradation of the target protein (Nishimura et al., 2009). Transcription of *CUP1* was not affected by auxin treatment (Figure S3A). Dynamics of Rsc2p-AID*-9Myc degradation was observed by western blotting (Figure S3C).

For the western blots and RT-qPCR, cells were grown exactly like SMT, but JF646 was not added. Copper induction was given in the tubes by adding 100 μM $CuSO_4$ directly to the culture media and shaking the tubes for exactly 10 min.

For smFISH, overnight grown culture was inoculated in 100 mL of fresh media at OD_{600} 0.2 and grown for 240 min in 500 mL flask. Cells were pelleted and resuspended in 35 mL of fresh CSM-LEU media and grown with aeration for 30 min in 500 mL flask. 8 mL samples were harvested as an uninduced condition and fixed with 2 mL of 16% formaldehyde. 100 μM $CuSO_4$ was added to the remaining culture and kept for shaking for exactly 10 min. 8 mL samples were harvested as an induced condition and fixed with 2 mL of 16% formaldehyde. smFISH for the *CUP1*-reporter mRNA was performed and quantified.

For the quantitative cell viability assay/copper resistance assay (Figure 3C and S1C), cells were grown to OD_{600} 0.9. Cell concentration was estimated in a hemocytometer. Cells were diluted to 500/mL^{-1} in 40 mL of autoclaved distilled water and placed in a sterile Petri dish (D = 90 mm). The cell suspension was plated with a pin replicator onto the plates with solid CSM media (DOBA, MP Biomedicals), containing either auxin (1 mM) and/or $CuSO_4$ (100 μM). Plates were incubated at 30°C for 72 hr and colonies were counted manually. Experiment was repeated thrice, values were normalized to maximum for each replicate and averaged. Error bars indicate standard error of the mean (SEM).

METHOD DETAILS

Chromatin immunoprecipitation (ChIP)

ChIP was performed as in Mehta et al., 2014 with modifications. Approximately 10^9 cells were used per sample (four IPs and an Input). Chromatin was cross-linked using 1% formaldehyde for 30 min at 25°C. Cells were washed twice with ice cold TBS (0.25 M Tris base, 1.37 M NaCl, 0.03 M KCl) and cell lysis was performed in 1.6 mL of lysis buffer (50 mM HEPES-KOH, pH 7.5, 140 mM KCl, 1 mM EDTA, 1% Triton X-100, 0.1% sodium deoxycholate, freshly added protease inhibitor cocktail from Roche) and equal volume of 0.5 mm glass beads (Scientific Industries) using MP FastPrep-24 bead beater (MP Biomedicals, 4 cycles of 40 s each with 5 min on watery ice in between). Chromatin was fragmented to an average fragment size of 200–500 base pairs using Diagenode Bioruptor (Diagenode) for 30 cycles of 30 s each at high setting. Sonicated lysates were centrifuged (14000 RPM for 10 min) to remove cell debris. Out of ~1.4 mL of clarified lysate, 100 μL lysate was stored at −20°C as an input (Whole Cell Extract, WCE) and two IPs of 600 μL each were rotated overnight at 4°C with the following beads/antibodies: 20 μL of GFP-TRAP-MA (ChromoTek, Cat no. gtma-20) for pulling down Ace1-3xGFP, 5 μg of Anti-Myc tag antibody (abcam, Cat no. ab9132) for pulling down Rsc2-AID*-9Myc, 5 μg of Anti-HaloTag antibody (Promega, G9281) for pulling down Ace1-HaloTag. Following overnight incubation with antibodies/beads, 20 μL of Protein A+G magnetic beads (Millipore-Sigma, Cat no. 16-663) were added to each tube for pulling down Rsc2-AID*-9Myc and Ace1-HaloTag and rotated at 4°C for 2 hr. The immunoprecipitated material was washed twice with 1 mL of IP wash buffer I (50 mM HEPES-KOH, pH 7.5, 150 mM NaCl, 1 mM EDTA, 0.1% sodium deoxycholate, 1% Triton X-100); once with 1 mL of IP wash buffer II (IP wash buffer I with 500 mM NaCl), once with 1 mL of IP wash buffer III (10 mM Tris pH 8.0, 250 mM LiCl, 0.5% NP-40, 0.5% sodium deoxycholate, 1 mM EDTA) and once with 1 mL of 1 × TE. The beads were resuspended in 100 μL of elution buffer (50 mM Tris, pH 8.0, 10 mM EDTA, 1% SDS) and incubated at 65°C for 15 min. The elution step was repeated in 50 μL of elution buffer and both the eluates were mixed to get the total eluate volume of 150 μL per IP and incubated overnight at 65°C for decrosslinking. As input control, 100 μL of WCE (stored at −20°C) was mixed with 50 μL of elution buffer and incubated overnight at 65°C for decrosslinking. DNA from all the samples (IPs and Inputs) were purified using Wizard SV Gel and PCR clean up system (Promega, Cat no. A9282) according to the manufacturer's instructions and eluted in 50 μL of elution buffer. qPCR was performed in duplicate using a Bio-Rad CFX96 machine in 20 μL SYBR Green reaction mixture (Bio-Rad, Cat no. 170-8882). T509 and T510 primer pair was used to amplify *pCUP1* locus (Table S3). Calculations for Enrichment/Input values (%) were

made using the following equations: $\Delta CT = CT(ChIP) - [CT(Input) - \log_E(Input\ dilution\ factor)]$, where CT is a Cycle Threshold, E is the specific primer efficiency value; Enrichment/Input (%) = $E^{-\Delta CT}$. All the ChIP experiments were performed at least twice, values were normalized to maximum for each repeat and averaged. Error bars indicate SEM. YTK1390 strain was used as a No Tag Control.

Quantitative RT-PCR (RT-qPCR)

RNA preparation was performed as described (Ball et al., 2016). cDNA was prepared using the iScript cDNA synthesis kit (BioRad, Cat no.: 1708891) starting with 1 mg of total RNA. Quantitative real-time PCR (qPCR) was performed as described (Ball et al., 2016). Primers used for the quantification of transcripts were T531, T532 for *CUP1*, and T1019, T1020 for *CUP1* reporter (Table S3). For normalization, the expression of the housekeeping gene *TUB1* or *ACT1* was quantified using primers T992, T993, or T1055, T1056, respectively (Table S3). To confirm the absence of contaminating genomic DNA in cDNA preparations, reverse transcriptase negative (-RT) samples were used as a control, which produced the Ct value difference of $\geq$ 10 cycles between "-RT" and "+RT" samples, indicating negligible amount of genomic DNA contamination in cDNA samples. mRNA extraction, cDNA synthesis and qPCR were repeated at least twice, and qPCR was performed in duplicates for each experiment. Error bars indicate SEM.

Protein concentration by western blots

Cells of YTK1649 were grown from OD_{600} 0.2 to 0.8 in 3 mL CSM-LEU media. Protein extraction and western blotting were performed by the standard procedure using anti-HA (1:3000 dilution, Roche Mouse Anti-HA (12CA5) Cat no. 11583816001), anti-c-Myc (1:3000 dilution, Roche Mouse Anti-c-Myc (9E10) Cat no. 11667149001) and anti-Tub2 (1:4500 dilution, Rabbit serum) antibodies. Protein extraction was repeated twice, values of band intensities (after background subtraction) were normalized to maximum and averaged. Error bars indicate SEM.

Quantification of Ace1p-GFP

To measure the nuclear brightness of Ace1p-GFP (Figure S3D) or the brightness of the individual arrays (Figure S2E), cells were imaged with the 100x 1.4 NA oil immersion objective using the FITC filter set (Ex 475/28; Em 525/48 Chroma Technology Corp) on a DeltaVision Elite imaging system (GE Healthcare) based on an Olympus IX71 inverted microscope (Olympus America) equipped with LED illumination and a sCMOS pco.edge camera (PCO AG, Kelheim), and controlled by SoftWoRX software. Z stacks of 9-11 focal planes were acquired with a Z step size of 350 - 400 nm, and XY pixel size of 65 nm (bit depth: 15-bit). Exposure was set to 150-300 ms. For the nuclear measurements, different fields of cells were collected. For the array measurements, videos with a 30 s time lapse were acquired. Measurements of the nuclear brightness or of the array brightness were performed in > 150 cells or 38 arrays, correspondingly. Fluorescence intensity was measured from the projection images using Metamorph (Molecular Devices). Average image background intensity was subtracted from the average intensity. In time-lapse videos brightness of the arrays was divided by the brightness of Ace1p in the nucleoplasm to correct for the photobleaching due to imaging. The brightness curves were normalized to the first time point, where no arrays were yet observed.

Custom-built Microscope for SMT

For SMT, we used a custom wide-field microscope capable of simultaneous imaging in three channels that is based on designs previously described (English and Singer, 2015; Morisaki et al., 2016). Briefly, three solid-state excitation lasers at wavelengths 488, 561, and 647 nm (OBIS, Coherent) are combined, expanded to provide more even illumination at the sample, and focused at the back focal plane of a 100x, 1.49 N.A., oil immersion objective (Olympus Scientific Solutions). To reduce background, HILO illumination (Tokunaga et al., 2008) is achieved by moving the radial position of the beam in the objective back aperture with a movable mirror, and the thickness of the excitation is adjusted by use of a manual diaphragm. Fluorescence emission is separated from scattered laser light by use of a quad-band dichroic (ZT405/488/561/647, Chroma Technology), and the emission bands are separated by two long-pass filters (T588lpxr, T660lpxr), and emission filters (525/50, 609/58 and 736/128, Semrock) before being focused on separate EMCCD cameras (iXon Ultra 888, Andor Technology), with 200 mm tube lenses. The combination of objective lens and tube lens results in a total magnification of 111x, corresponding to a XY pixel size of 117 nm. The sample is held on a motorized XY translation stage with piezo Z (PZ-2000 XYZ, Applied Scientific Instrumentation), which is mounted on a Rapid Automated Modular Microscope System (RAMM, Applied Scientific Instrumentation). All lasers and cameras are synchronized using a microcontroller board (Arduino UNO), and images are collected using the open source microscope control software, Micro-Manager (Edelstein et al., 2014).

SMT: staining, imaging, and quantification

The protein of interest (Ace1p-HaloTag or Rsc2p-HaloTag) was labeled with JF_{646} at 0.5 nM concentration as described in (Ball et al., 2016). Live cells were imaged under CSM+100 μM $CuSO_4$ agarose pads using LabTek II chambers. We simultaneously imaged GFP and JF_{646} channels on the custom-built imaging system at room temperature. Time-lapse videos were acquired as 16-bit single focal plane images with 30 ms laser irradiation (Ex: 100 μW 488 nm; Ex: 1 mW 647nm) and 200 ms time interval for a total of 2 min.

In our experiments, we were interested in assaying the TF binding to a specific promoter. Tracking of Ace1p in the whole nucleus may measure binding not only to *CUP1* but also to the other four promoters that are regulated by Ace1p (Gross et al., 2000). To ensure that we are measuring the TF binding either at *CUP1* promoter, or at the region where there are reliably no known REs for Ace1p, Ace1p-HaloTag-JF_{646} or Rsc2p-HaloTag-JF_{646} were tracked only at the ROI defined by the green spot of the *CUP1* or *lacO* array.

We compared binding over the *CUP1* array to binding over *lacO* (Figure 1) to offset any unforeseen effects of measuring the region smaller than the whole nucleus. We also tracked Ace1p in the whole nucleus and compared it with Ace1p at the *CUP1* array from the same cells (Figure S2B). We found that the parameters for non-specific binding remain the same, hence tracking volume doesn't affect non-specific binding. SMT for Figures 1, 2 and 6 were performed with ROIs manually drawn around individual arrays based on the GFP images. The sizes of the ROIs were similar for Rsc2p^{+} and Rsc2p^{-}, with mean areas of 0.93 ± 0.03 (SEM) μm^2, and 1.16 ± 0.05 μm^2, respectively (p value = 0.009, by Kolmogorov-Smirnov test), while the *lacO* arrays were slightly smaller with a mean area of 0.5 ± 0.2 μm^2. This variability may be due to the different level of decompactization of the DNA. Heavily transcribed arrays of loci may become bigger due to looping out of the transcribed DNA. In addition, it is known that in RSC2^{-} cells the sister chromatids are prematurely separated, which may contribute to the larger perceived size of the array.

Tracking was performed automatically with the MATLAB-based (The Mathworks). Track Record software (freely available at https://sourceforge.net/projects/single-molecule-tracking). Track Record links molecule positions in two consecutive planes using a nearest-neighbor approach (Mazza et al., 2012). Molecules are considered bound if they move less than r_{max} = 220 nm from one frame to the next (Ball et al., 2016) for at least N_{min} = 4 frames (Figure S2A). Assuming a moderate diffusion coefficient, D_f, of 0.5 $\mu m^2/s$, with our frame interval, Δt, of 200 ms, these parameters reduce the probability that a freely diffusing molecule will be classified as bound to p = 1.7 × 10^{-4} based on the equation (Mazza et al., 2012):

$$P = \left(1 - e^{-\frac{r_{max}^2}{4D_f \Delta t}}\right)^{N_{min}}$$

The total bound fraction, C_{eq}, is found by summing up the number of time-points in all bound track segments and dividing by the total number of particles found. The fraction of diffusing molecules is therefore given by (1- C_{eq}).

The survival distribution (1 – CDF) is generated from the bound track segments. Photobleaching is measured within each experiment by counting the number of particles found in each frame, and fitting to a bi-exponential decay by least-squares. The survival distribution is then divided by the best-fit photobleaching curve to correct for photobleaching and normalized to the total bound fraction C_{eq}. This procedure was validated in Monte Carlo simulations (Ball et al., 2016).

Mean residence times and the fraction of total molecules within each population were estimated by fitting by least-squares the photobleaching-corrected survival plots to mono- and bi-exponential functions. Typically, the plots are fit best with bi-exponential decay. The fastest (short-residence) component represents nonspecific binding to DNA, i.e., sampling the DNA for binding sites. See Ball et al., 2016 for further discussion of nonspecific binding of Ace1p. The second (longer-residence) component represents binding to specific RE (specific binding). The third sub-population shown in Figures 1 and 2 arises from those track segments that were considered unbound based on the criteria described above, and particles that were not tracked and represent diffusing molecules. Diffusion coefficients for all the fractions for Ace1p and Rsc2p are presented in Figure S2C. Due to the long exposure time relative to molecular diffusion, we likely underestimate the number of freely diffusing TFs. However, the focus of this study is on the bound molecules. Comparisons between the various strains remain valid, as all were imaged under the same conditions.

The track analysis method that we adopted (fitting of the Cumulative Distribution Function, or CDF) is based on survival rates (Morisaki et al., 2014; Loffreda et al., 2017; Presman et al., 2017). Other methods available are Probability Density Function (PDF) fitting (Das et al., 2009; Liao et al., 2015) or variational Bayes Single-particle tracking (vbSPT, Persson et al., 2013). As evaluated in detail in Presman et al., 2017, CDF fitting provides better estimates for the residence times of bound molecules than PDF fitting and thus it is a better match for our scientific focus on bound, rather than diffusing TF. In this paper we further evaluated comparative applicability of CDF fitting and vbSPT specifically to our data range. We generated artificial tracks based on parameters extracted from SMT of Ace1p in RSC^{+} cells activated by Cu^{2+}, i.e., based on data of Figures 1C and 1D. Then we applied CDF fitting and vbSPT analysis to the simulated tracks (Figure S2D). Ideally, a good analysis method would return the parameters close to those used to simulate the tracks. The vbSPT analysis, as opposed to CDF fitting, returned dramatically incorrect residence times for both short-residence and long-residence molecules. Interestingly, correct estimates for the fraction of diffusing molecules are returned by vbSPT only for the homogeneous population (*lacO*) but this fraction is grossly underestimated if a second, specifically bound fraction is present (*CUP1* array). Thus, we adopted CDF fitting for our data.

Quantification by survival rates adopted in this paper assumes that the Ace1p binding is in steady state. We ensured that we perform SMT at the Ace1p binding-unbinding equilibrium. Ace1p-GFP binding measured by fluorescent intensity of the array indicates that for about ~5 min it remains relatively constant, i.e., the system is in steady state. This plateau in fluorescent intensity is preceded by a rapid rise in fluorescence after the addition of copper and is also followed by a rapid decline in fluorescence (Figure S2E). These phases of fluorescence increase or decrease were avoided in all of our SMT measurements, as we started measurements after 5 min of Cu activation and performed them on bright arrays for 2 min total time.

smFISH: staining, imaging, and quantification

By smFISH one can observe mature transcripts and identify *CUP1* transcription sites (TS) containing nascent mRNA. Due to the multiple copies of *CUP1* in the genome, smFISH of native *CUP1* does not allow for the monitoring of the transcriptional output of an individual gene in the array. We therefore replaced one ORF within the array with a synthetic *CUP1*-reporter. This reporter was derived from the scrambled sequence of the rat Glucocorticoid Receptor (GR), to which 8 MS2 binding sites were appended (Figures 4A and

S4). As the sequence of this reporter is unique, its transcripts may be observed separately from the transcripts from the remaining copies of *CUP1*. The sequence contains multiple stop codons and cannot be translated, preventing any toxicity from the expressed protein.

Cells were stained with TAMRA-labeled custom-made Stellaris smFISH probes (synthesized by LGC Biosearch Technologies) specific for the transcripts of *CUP1*-reporter (see Figure S4 for the position of the probes). Briefly, we fixed the cells with 3.7% formaldehyde after 10 min of Cu induction (or control cells with or without Cu/Auxin induction). Fixed cells were stained with smFISH probes as described in (Raj and Tyagi, 2010). After staining, cells were resuspended in 30 μl of Antifade buffer with glucose oxidase and catalase. 5 μl cell suspension was layered on a poly-L-lysine coated cover glass. A drop of Vectashield mounting medium (+DAPI, Vector Laboratories) was placed in the center of a glass slide and this slide was placed upside down on top of the coverglass and pressed gently to mix the cells in suspension with Vectashield. Cells were imaged with the 100x 1.4 NA oil immersion objective on a DeltaVision Elite imaging system. Z stacks of 50 focal planes were acquired with a step size of 200 nm, and XY pixel size of 65 nm (bit depth: 15-bit). Images of ~500 cells were captured using filter sets for DAPI (Ex 390/18; Em 435/48) and TRITC (Ex 542/27; Em 597/45, Chroma Technology Corp, Bellows Falls, VT) and deconvolved. Exposure was set to 300 ms for TRITC channel and 10 ms for DAPI channel.

Images were analyzed using FISH-Quant software (Mueller et al., 2013). Mature RNAs for measurements were identified in deconvolved images as 3D Gaussian spots with intensity higher than an arbitrary threshold, which was held constant for all acquisitions belonging to the same experiment. The number of mRNA per cell, number of nascent transcripts per transcription site and the brightness of the individual mRNA spot were measured from raw images. The spots that we measured were indeed single molecules of mRNA, because of the narrow distribution of the brightness of the individual mRNA spots (Figure S5A). Quantification of the transcription of the reporter by smFISH and by RT-qPCR demonstrate that both methods applied to the same reporter register the same proportion in transcription reduction in absence of RSC. Thus, smFISH is an adequate method for quantification of the expression of the *CUP1* reporter (Figure S5B). Transcriptional output of the *CUP1* reporter inserted under a natural *CUP1* promoter is representative of the other *CUP1* genes of the same array because quantification of *CUP1* reporter transcription provides results similar to those obtained for the whole array of the endogenous *CUP1* in the same culture (Figure S5C). Experiment was repeated twice and error bars indicate SEM (Figures S5B and S5C).

mRNA degradation rate

The degradation rate of the *CUP1* reporter mRNA was measured in YTK1649 by smFISH as above. 200 cells were measured every 5 min after washing out the Cu^{2+} from the growth medium (Figure S5D, upper panel). The degradation rate of the endogenous *CUP1* was measured by RT-qPCR, as transcription of ten copies of *CUP1* results in very large amounts of mature mRNA in the cytoplasm uncountable by smFISH due to overlapping spots. Cells for RT-qPCR were harvested every 5 min after washing out Cu^{2+}. In both cases, the degradation rate was calculated by fitting by least-squares the mean mRNA values of the time-course to a mono-exponential decay (middle and lower panel). We can measure the activity of individual promoters only by reporter transcription, therefore we have to input the degradation rate of the reporter into our model. The endogenous *CUP1* mRNA is more stable than mRNA of the reporter (12.1 ± 3.4 min versus 8.2 ± 1.6 min). However, this difference does not affect our conclusions. If the degradation rate changes, then all the parameters would be scaled proportionally, but this would not affect the ratio between those.

CUP1 nucleosome occupancy by MNase-seq

Nucleosome occupancy was determined for the following four conditions: (1) $Rsc2^{+}$ (No Auxin), no Cu activation, (2) $Rsc2^{+}$ (No Auxin), with Cu activation, (3) $Rsc2^{-}$ (With Auxin), no Cu activation, (4) $Rsc2^{-}$ (With Auxin), with Cu activation. Cells of haploid YTK1460 were grown overnight in 10 mL CSM-URA and diluted to OD_{600} 0.2 in 400 mL of the fresh CSM-URA. Cells were grown for 270 min to OD_{600} 0.8 at 30°C and 230 RPM. For auxin-induced Rsc2p depletion IAA was added to the culture media 240 min before Cu treatment to a final concentration of 1 mM. For copper activation, cells were treated for 10 min with 100 and 4 μM $CuSO_4$. Cells were harvested by filtering the culture through 0.45 μm Nalgene Rapid Flow Nylon Filter unit (Thermo Fisher Scientific, Cat no. 151-4045) and washing the cells with ice-cold autoclaved distilled water into 50 mL Falcon tubes. Pellets were frozen at −80°C.

Nuclei were prepared and digested by MNase as described (Cole et al., 2012). DNA was purified from digests composed predominantly of mono-nucleosomes. Nucleosomal DNA (0.5 - 1 μg) was repaired using the PreCR repair kit (NEB M0309). Paired-end libraries were prepared from the repaired DNA using NEB Illumina kits E7370 and E7335, with 7 PCR cycles, according to the manufacturer's instructions. The samples were multiplexed and sequenced by an Illumina HiSeq2500 (2x 50 nt reads). Nucleosome occupancy plots were constructed as described (Chereji et al., 2017). The sequencing data from this study, including biological replicates, have been submitted to the NCBI Gene expression Omnibus under accession number GEO: GSE112685.

The yeast genome sequence used for alignment includes two identical copies of the *CUP1* locus, named *CUP1-1* and *CUP1-2*. Our data show that the coverage of *CUP1* locus is about 5X of the flanking sequences, indicating that there are about ten *CUP1* repeats in this strain. When cells are depleted of Rsc2p, the Transcription Start Site (TSS), initiation element and TATA box show decreased nucleosome occupancy, whereas the UAS elements show a small increase in nucleosome occupancy. The latter effect is primarily due to an upstream shift of ~40 bp in the position of a particular +1 nucleosome such that it now covers the distal UAS as well as the proximal UAS. The net effect of Rsc2 is to increase the accessibility of the distal UAS.

QUANTIFICATION AND STATISTICAL ANALYSIS

Relationship between SMT parameters

In the main text, we use a simplified system (Equation 1) to illustrate the interdependence of off-rate (k_{off}), pseudo "on"-rate (k^*_{on}), and bound fraction (C_{eq}). When a TF transiently binds to random DNA sequences and more strongly to its target sequence, Equation 1 becomes (Loffreda et al., 2017)

$$C_{eq} = \frac{\frac{F_S}{k_{off_S}} + \frac{1-F_S}{k_{off_N}}}{\frac{F_S}{k_{off_S}} + \frac{1-F_S}{k_{off_N}} + \frac{1}{k^*_{on_S} + k^*_{on_N}}}, \quad \text{Equation M1}$$

where F_S is the fraction of bound molecules that are associated to their target sequence, k^*_{onS}, is the pseudo-"on" rate for the specific binding, k^*_{onN} is the pseudo-"on" rate for non-specific binding, and k_{offS} and k_{offN} are the "off" rates for the specific and non-specific bound molecules, respectively.

The fraction of bound molecules that are at the target sequence can also be expressed solely in terms of the pseudo "on"-rates

$$F_S = \frac{k^*_{on_S}}{k^*_{on_S} + k^*_{on_N}}. \quad \text{Equation M2}$$

Solving Eq M1 and M2 for k^*_{onS} and noting that the average lifetime of all bound molecules, $\bar{\tau} = F_S\tau_S + (1-F_S)\tau_N = F_S/k_{off_S} + 1 - F_S/k_{off_N}$, the pseudo "on"-rate for the specifically bound population can be calculated based on the values obtained from fitting the SMT data for total bound fraction, C_{eq}, slow-bound fraction, F_S, and the lifetimes of the two states, τ_S and τ_N

$$k^*_{on_S} = \frac{C_{eq}F_S}{(1-C_{eq})\bar{\tau}}. \quad \text{Equation M3}$$

In addition, if we note that $\tau_{3D} = \frac{1}{k^*_{on_S} + k^*_{on_N}}$ defines the average time between two binding events, Equation M1 becomes

$$C_{eq} = \frac{\bar{\tau}}{\bar{\tau} + \tau_{3D}}. \quad \text{Equation M4}$$

Rearranging Eq. M4 yields

$$\tau_{3D} = \frac{\bar{\tau}(1-C_{eq})}{C_{eq}}. \quad \text{Equation M5}$$

On average, it will take $1/F_S$ trials for the TF to locate its target sequence, with each trial requiring a time equal to $\tau_{3D} + \tau_N$, with the exception of the final trial, which requires only τ_{3D}. The total time required to locate the target sequence is therefore

$$\tau_{search} = \frac{\tau_{3D}}{F_S} + \frac{(1-F_S)\tau_N}{F_S}. \quad \text{Equation M6}$$

Note that if there is only specific binding, $F_S = 1$, and therefore $\tau_{search} = \tau_{3D} = \tau_S(1-C_{eq})/C_{eq}$, which is a rearranged version of Equation 1 from the main text.

Estimating fraction of non-active cells

The diploid YTK1649 cells were treated the same as described above for smFISH without the addition of Cu^{2+} to obtain the basal transcription output of *CUP1*. In this control group, cells contain on average very few mature mRNA of *CUP1*-reporter (0.46 ± 0.03 (SEM)) per cell, with a maximum of 8. Cells that do not contain any mRNA constitute 67.2% of the whole population (Figures 4D and 4E). The histogram of mature mRNA is fit well to a Poisson distribution with a mean of 0.46, indicating that basal expression of *CUP1* is governed by random, uncoordinated initiation, rather than a bursting behavior.

To estimate the fraction of non-active cells, F_{nt}, in the Cu^{2+}-treated populations of $Rsc2^+$ and $Rsc2^-$, the initial part of each distribution (cells containing three or fewer transcripts) was fit to a scaled Poisson with the mean, λ, fixed at the mean of the control cells (0.46 transcripts/cell), and varying only the scaling parameter α:

$$F_{nt}(k) = \alpha\frac{\lambda^k e^{-\lambda}}{k!}. \quad \text{Equation M7}$$

The scaled Poisson with a fixed mean was used instead of directly fitting to a separate Poisson distribution to avoid overestimation of F_{nt} due to active cells with low mRNA levels.

Estimation of $S_{Equation}$ and k_{on}

If we assume that binding of Ace1p to any of the four binding sites in the *CUP1* gene occurs equally and independently and results in transcription, then we can relate F_{nt} to the probability, P, that any one RE is available:

$$F_{nt} = (1 - P)^4. \quad \text{Equation M8}$$

By knowing how many RE are available for each gene and assuming a nuclear radius of 1 μm, corresponding to a volume of $V = 4.19 \times 10^{-15}$ l, we may calculate S_{eq}:

$$S_{eq} = \frac{n}{N_A V}, \quad \text{Equation M9}$$

where N_A is Avogadro's constant.

Monte Carlo Simulations of TF binding

To examine the relative impact of changes to the RE availability or "on" rate on transcriptional output, we performed Monte Carlo simulations of a random telegraph model in MATLAB (The Mathworks) using Gillespie's SSA algorithm (Gillespie, 1977). Promoters of *CUP1* contain four REs for Ace1p (Shen et al., 2001). Thus, we assigned four REs to simulated *CUP1* promoters, and we assumed that binding of Ace1p to any of the four REs resulted in equally efficient transcription. The simulation of each cell was initialized with a fixed fraction of available binding sites, by selecting a binomially distributed random number with the number of trials equal to the total binding sites, and the probability equal to the specified fraction of available sites. Once initialized, the availability of each site remained fixed throughout the time-course. Each available RE was either unbound or bound by a TF and switched to these states with exponentially distributed waiting times with means $1/k_{off}$ and $1/k^*_{on}$, respectively. When any of the RE was in the "ON" state, transcription was initiated with an exponentially distributed waiting time with mean, $1/k_{tx}$. At all time-points of the simulation, each transcript was classified as either nascent if it had existed for less than the production time (t_{prod}), or mature if it had existed for longer. Mature transcripts could degrade with an exponentially distributed lifetime with mean of $1/k_{deg}$.

When assessing the role of the RE availability, probabilities between 1%–99% were set in the model, while keeping all other parameters fixed. Similarly, to determine the impact of the "on" rate, values between 1.35×10^8 and 5.4×10^8 M^{-1} s^{-1} were used with other parameters held constant. For clarity, we plot the mean number of transcripts in active cells versus the fraction of non-active cells of these scans (Figure S6A). Neither of the curves fits the experimental data. Although the experimental data (black dots) are close to the simulated plot for the variability of RE (green curve), the difference between the mean mRNA value for $Rsc2^+$ and the value on the green line for the same fraction of non-active cells is statistically significant based on a Kolmogorov-Smirnov test (p value < 0.001). We also varied the "on" rate over a greater range (from $10^4 - 10^{12}$ $M^{-1}s^{-1}$) to determine if a much faster (or slower) "on" rate could recapitulate the experimentally obtained mean mRNA in active cells (Figure S6B, black line), and the fraction of non-active cells (Figure S6C, black line). In this case, all REs were made available by setting the probability to 1. The result of this parameter scan showed that there exist 3 regimes: (1) with an "on" rate below $\sim 10^7$ $M^{-1}s^{-1}$ only the fraction of non-active cells changed, while the mean number of mRNAs in active cells remained fixed at a very low abundance (< 2 mRNAs/cell); (2) between $\sim 10^7$- $\sim 10^{10}$ $M^{-1}s^{-1}$, only the mean number of mRNA in active cells changes; (3) above 10^{10} $M^{-1}s^{-1}$, both the fraction of non-active cells, and the mean number of mRNA in active cells remain constant. Increasing the number of bound REs required to start transcription to two (red curves in Figures S6B and S6C) or three (blue curves in Figures S6B and S6C) only changes the value of k_{on} required to obtain the observed mean mRNA in active cells (~20 per cell), but still does not provide a regime where only the fraction of inactive cells changes. Therefore, it is not possible to simultaneously obtain different fractions of active cells and the same (high) mean number of mRNA by changing only the "on" rate.

To further test that, we looked at the impact of changing the probability of RE availability (P) alone, or of all three parameters: P, k_{on}, and k_{off}. Experimentally, for *CUP1* we observe that in $Rsc2^+$ the fraction of the cells with non-activated *CUP1* decreases, and the trancriptional output of activated *CUP1* stays the same: 19 ± 0.5 (SEM) for $Rsc2^-$ and 18 ± 0.4 for $Rsc2^+$. Simulations show that maintaining the same level of output requires changes not only in P but also in k_{on}, and $k_{off.}$. Specifically, if a gene contains four REs (such as *CUP1*), then increasing only P from 0.28 to 0.38 resulted not only in a reduction in the fraction of the cells with non-activated *CUP1* similar to that observed in experimental data, but also increased the mean simulated transcriptional output of active cells, which contradicts the experimental data (Figure S6D). Thus, we cannot reproduce this result if only the availability of RE changes. Only by increasing P, k_{on}, and k_{off}, were we able to see something similar to our experiments (Figure S6E). Namely, the fraction of cells with non-activated *CUP1* decreases the same as in Figure S6D, but the mean mRNA in cells with active *CUP1* is relatively unchanged. In contrast, when a gene contains only a single RE, the results of changing only P (figure S6F), or changing P, k_{on}, and k_{off} (Figure S6G) are indistinguishable.

Our model also indicates that all four REs for *CUP1* actively participate in binding. Assuming the gene contains four RE, simulations of the distribution of mRNA/cell are similar to the experimental (compare Figures S6D and S6E with Figure 5C). In contrast, if the gene is assumed to contain only one RE, the distribution of mRNA/cell is much narrower than experimental distributions (compare Figures S6F and S6G with Figure 5C), which provides further evidence that *CUP1* gene contains multiple (most likely four) RE.

Finally, we tested the assumptions of our model. We assume that all four binding sites for Ace1p in the *CUP1* promoter are equal, and productive binding of at least one Ace1p converts the gene to "ON" state. Our assumption that Ace1p does not bind

cooperatively is based on the following: (a) a single binding site is enough to activate other genes of the copper regulon by Ace1p (Peña et al., 1998); (b) Ace1p does not dimerize prior to binding (Buchman et al., 1990). We decided to test the outcome of fitting of experimental data based on a requirement for transcription of multiple bound Ace1p molecules. Assuming a requirement for multiple binding events dramatically affected predictions for the "on" rate. In the case where there is no cooperativity and only a single RE binding is sufficient, the predicted "on" rate is $2.7 \times 10^8\ M^{-1}s^{-1}$. If transcription of *CUP1* requires two REs to be occupied by TFs the returned "on" rate will be ~3 × faster ($8 \times 10^8\ M^{-1}s^{-1}$), and ~100 × faster ($3 \times 10^{10}\ M^{-1}s^{-1}$) if *CUP1* requires three REs to be occupied by TFs to begin the transcription. The high "on" rate found assuming multiple occupancy is in agreement with measurements of the lac repressor in bacteria cells (Riggs et al., 1970). However, most studies of DNA-binding proteins have found rates that are on the order of $10^8\ M^{-1}s^{-1}$ (Kim et al., 1987; Kleinschmidt et al., 1988; Hoopes et al., 1992). We therefore chose the model with a requirement of a single RE-TF complex. Importantly, regardless of the required number of RE-TF complexes our conclusion remains unchanged: observed behavior, namely, that the number of active cells increases with Rsc2p, but the mean number of mRNA in active cells stays the same, may be explained only by simultaneous changes both in "on" rate and RE availability (Figure S6B). Thus, simulations showed that our data can be fit well without the addition of cooperative binding. However, we do not exclude cooperative binding completely. We just argue that cooperative binding is not necessary to explain our results.

Our model takes into account the summary result of the extrinsic and intrinsic noise, although it is not possible for us to completely separate these sources of noise as we only observe the output of one gene (*CUP1* reporter) per cell. Assuming four REs, we model a system that displays a combination of extrinsic and intrinsic noise. The cell to cell variability in the model with four REs arises because in every cell, each of the four REs are either open or closed and remain in that state throughout the simulation. In a real cell this would lead to intrinsic variation between several copies of *CUP1*, which we cannot observe. However, in the model it results in different simulated cells having a different number of available REs and thus in extrinsic variation. A cell with more available REs will have a higher probability of binding a TF, and therefore produce more mRNA. In contrast, when only a single RE is present, each cell either has one available RE or none. Therefore, all active cells behave more similarly, and this situation models a system with only intrinsic noise. Based on comparison of the distributions in Figures S6E and S6G, the *CUP1* system displays both intrinsic and extrinsic noise. When the model includes 4 REs, we accurately reproduce the variability in the experimental data as characterized by the Fano factor (ratio of variance to mean). For $Rsc2^+$, the Fano factor of active cells is 6.1, while for $Rsc2^-$ it is 8.8. If the model only uses a single RE, the Fano factor is reduced to 1.8, which is close to Poisson-like noise (Fano factor = 1), and therefore indicative of purely intrinsic noise. Therefore, as four REs allow us to fit the data much better than one RE, it indicates that in experimental data we observe a mix of extrinsic and intrinsic noise, although the relative impact of intrinsic and extrinsic noise cannot be derived from the existing experimental data for the single reporter.

Curve-fitting of mature transcript distributions

We fit the mature mRNA distributions of the *CUP1*-reporter obtained by smFISH for both $Rsc2^+$ and $Rsc2^-$ using the above random telegraph model. During the fitting, k_{off} was held constant at the appropriate value: 0.19 for $Rsc2^-$; 0.46 for $Rsc2^+$, while S_{eq} and k_{on} were kept at the values described above, and the mRNA degradation rate was a constant obtained by measuring a smFISH time-course on fixed cells (Figure S3C). We then extracted k_{tx} and t_{prod} following the fitting strategy of (Senecal et al., 2014). Briefly, we used a custom random sampling method to explore parameter space, in which new possible parameters were selected to be close to linear combinations of previously found well-fitting parameters. Experimental mRNA distributions were compared to the model using the sum of the squared residuals. This process was repeated until 1000 parameter sets were obtained, and we report the mean and 95% confidence intervals of the best-fitting parameters. Table 1 shows the values of all parameters used to obtain the fits for the data shown in Figure 5C.

We then used the primary parameters from the model to obtain the characteristics of the transcriptional bursts. The bursting dynamics of transcription are typically characterized by the burst duration, $D = k_{off}^{-1}$, which is the average time the gene is ON, the frequency, $f = k_{on}^{*}k_{off}/k_{on}^{*} + k_{off}$, which is how often the gene turns on, and the amplitude, $A = k_{tx}/k_{off}$, which is the average number of transcripts produced in a single burst. A schematic representation of the model parameters and burst characteristics is presented in Figures 5B and 5D.

DATA AND SOFTWARE AVAILABILITY

The sequencing data for MNase-seq experiments, including biological replicates, have been submitted to the NCBI Gene expression Omnibus under accession number GEO: GSE112685.

Original images of SMT, smFISH and western blot are uploaded to Mendeley Data (for SMT and smFISH, only two images of each experimental condition were uploaded due to database size limitations) (https://doi.org/10.17632/hp9bwtnbgc.1).

TrackRecord (MatlabTrack_v5.4.4) can be downloaded from https://sourceforge.net/projects/single-molecule-tracking.